Quaternary Science Reviews 182 (2018) 175–190

Contents lists available at ScienceDirect

Quaternary Science Reviews

journal homepage: www.elsevier.com/locate/quascirev

Aeolian stratigraphy describes ice-age paleoenvironments in unglaciated Arctic Alaska

Benjamin V. Gaglioti [a, *], Daniel H. Mann [b], Pamela Groves [c], Michael L. Kunz [d], Louise M. Farquharson [b], Richard E. Reanier [e], Benjamin M. Jones [f], Matthew J. Wooller [g]

[a] Lamont-Doherty Earth Observatory of Columbia University, 61 Route 9w, Palisades, NY 10964, USA
[b] Department of Geosciences, University of Alaska Fairbanks, 900 Yukon Dr., Fairbanks, AK 99775, USA
[c] Institute of Arctic Biology, University of Alaska Fairbanks, 902 North Koyukuk Dr., Fairbanks, AK 99775, USA
[d] School of Natural Resources and Extension, University of Alaska Fairbanks, P.O. Box 757140, Fairbanks, AK 99775, USA
[e] Reanier & Associates Inc., 1215 SW 170th St., Seattle, WA 98166, USA
[f] Alaska Science Center, US Geological Survey, 4210 University Dr., Anchorage, AK 99508, USA
[g] Water and Environmental Research Center & School of Fisheries and Ocean Sciences, University of Alaska Fairbanks, 306 Tanana Dr., Fairbanks, AK 99775, USA

ARTICLE INFO

Article history:
Received 5 July 2017
Received in revised form
4 January 2018
Accepted 5 January 2018

Keywords:
Ice age
Arctic
Alaska
North slope
Pleistocene
Loess
Permafrost
Yedoma
Sand sheet
Sand sea
Paleoenvironments
Stratigraphy
Mammoth steppe

ABSTRACT

Terrestrial paleoenvironmental records with high dating resolution extending into the last ice age are rare from the western Arctic. Such records can test the synchronicity and extent of ice-age climatic events and define how Arctic landscapes respond to rapid climate changes. Here we describe the stratigraphy and sedimentology of a *yedoma* deposit in Arctic Alaska (the Carter Section) dating to between 37,000 and 9000 calibrated radiocarbon years BP (37–9 ka) and containing detailed records of loess and sand-sheet sedimentation, soil development, carbon storage, and permafrost dynamics. Alternation between sand-sheet and loess deposition provides a proxy for the extent and activity of the Ikpikpuk Sand Sea (ISS), a large dune field located immediately upwind. Warm, moist interstadial times (ca. 37, 36.3–32.5, and 15–13 ka) triggered floodplain aggradation, permafrost thaw, reduced loess deposition, increased vegetation cover, and rapid soil development accompanied by enhanced carbon storage. During the Last Glacial Maximum (LGM, ca. 28–18 ka), rapid loess deposition took place on a landscape where vegetation was sparse and non-woody. The most intense aeolian activity occurred after the LGM between ca. 18 and 15 ka when sand sheets fringing the ISS expanded over the site, possibly in response to increasingly droughty conditions as summers warmed and active layers deepened. With the exception of this lagged LGM response, the record of aeolian activity at the Carter Section correlates with other paleoenvironmental records from unglaciated Siberia and Alaska. Overall, rapid shifts in geomorphology, soils, vegetation, and permafrost portray an ice-age landscape where, in contrast to the Holocene, environmental change was chronic and dominated by aeolian processes.

1. Introduction

High resolution, paleo-environmental reconstructions of terrestrial Arctic ecosystems during the last ice age are relatively rare, despite the fact large parts of the Arctic remained unglaciated and today contain rich sedimentary archives of paleoenvironmental data (e.g., Brigham-Grette et al., 2007; Murton et al., 2015). Consequently, our understanding of how Late Pleistocene climate changes affected terrestrial Arctic ecosystems is limited compared to temperate ones, which is unfortunate because the Arctic is now on the frontline of climate change, and past ecosystem responses to climate change provide insights into how Arctic ecosystems may respond in the future.

One such unglaciated, Arctic region now experiencing high rates of climate change is Alaska's North Slope (Fig. 1) (Hinzman et al., 2005). Because it borders the Arctic Ocean, the North Slope's climate is closely linked to sea-ice dynamics (Bhatt et al., 2010; Wendler et al., 2010; Gaglioti et al., 2017) and so is subject to polar amplification of climate change (Miller et al., 2010). What were the nature and timing of landscape changes on Alaska's North Slope

* Corresponding author.
E-mail address: bengaglioti@gmail.com (B.V. Gaglioti).

https://doi.org/10.1016/j.quascirev.2018.01.002
0277-3791/

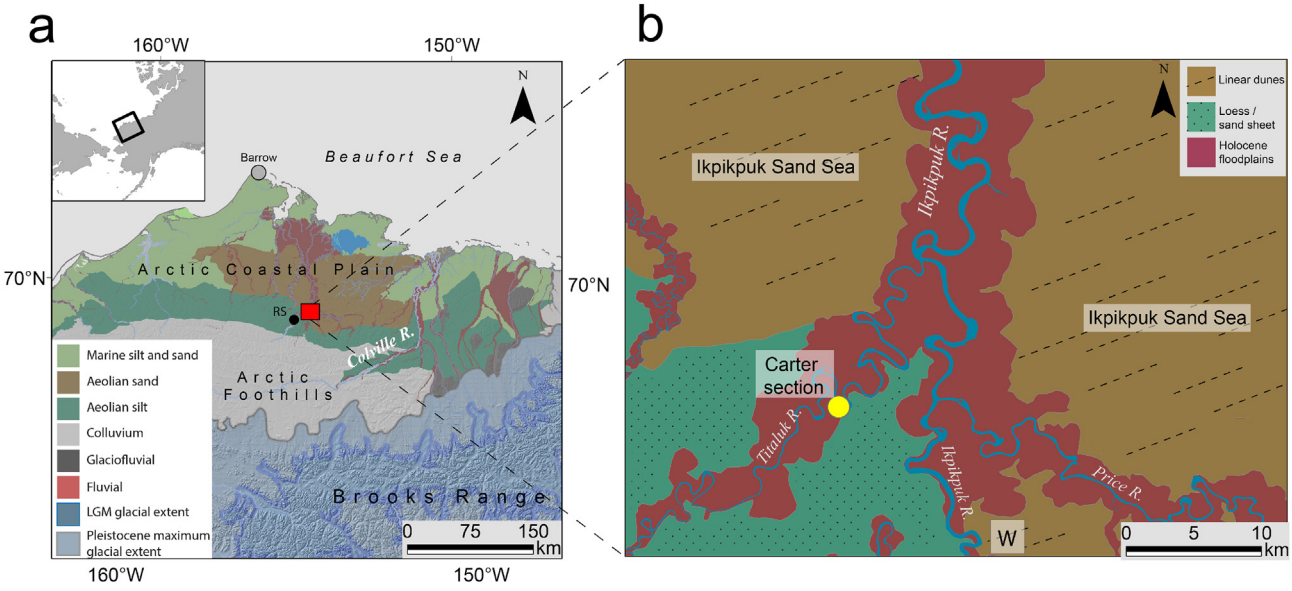

Fig. 1. a) Surficial geology of Alaska's North Slope (Farquharson et al. (2016). 'RS' is the Russian Section, 22 km upstream of the Carter Section. b) The southwest margin of the now-stabilized Ikpikpuk Sand Sea. The Carter Section lies in the boundary zone between sand-sheet and loess deposition. Wind data collected at location 'W'.

during the last ice age, and how were they different from today's? We address these questions by reconstructing the last 40 ka of changes in geomorphology, soils, and permafrost in a closely-dated stratigraphic section located adjacent to the now stabilized Ikpikpuk Sand Sea (ISS) (Fig. 1).

The Carter Section is a 2-km-long, 50-m-high cutbank of the Titaluk River located downwind of the southwestern margin of the ISS (Figs. 1 and 2). L. David Carter of the U.S. Geological Survey discovered the exposure in the 1980s and identified it as a yedoma deposit whose sediment was derived from the ISS (Carter, 1988; Carter and Galloway, 1993). "Yedoma" is frozen, fine-grained sediment of aeolian origin that often contains syngenetic ice wedges and significant amounts of organic carbon (Kanevskiy et al., 2011; Murton et al., 2015). Yedoma blankets large regions of Siberia, Alaska, and the Yukon that were not glaciated during the last ice age (Murton et al., 2015). Because it was often deposited gradually and frozen syngenetically, yedoma, like that exposed in the Carter Section, can provide valuable archives of paleoenvironmental information (Murton et al., 2015). The Carter Section is one of just several large, yedoma sections currently exposed on the North Slope, another being the Itkillik River Section located 150 km to the southeast in a different geomorphic setting (Kanevskiy et al., 2011; Lapointe et al., 2017) (Section 5.3.2).

2. Regional setting

2.1. Climate, vegetation, permafrost

Alaska's North Slope lies above the Arctic Circle between the Brooks Range and the Arctic Ocean (Wahrhaftig, 1965) (Fig. 1). Mean July temperatures increase from 4° to 12 °C from the Beaufort Sea coast to the Brooks Range (Zhang et al., 1996). Much of the North Slope receives only 200–320 mm of annual precipitation and has a semi-arid climate (Newman and Branton, 1972). Mean annual precipitation increases to the south, away from the Arctic Ocean (Zhang et al., 1996). About half the annual precipitation falls as snow, which covers the ground for 8–9 months of the year. As a consequence of these gradients in temperature and precipitation, primary productivity is lower, woody vegetation is less abundant, and soils are colder with increasing distance north of the Brooks Range (Nelson et al., 1998; Walker et al., 2003).

Today the North Slope supports Low Arctic, tundra vegetation consisting of sedges (Cyperaceae), mosses, and dwarf-shrubs (e.g., Ericaceae) growing in lowland and low-relief areas, and tussock-forming sedges (e.g. *Eriophorum vaginatum* L.), dwarf-shrubs, and mosses growing in uplands (Walker et al., 2005, 2011). The entire region is underlain by continuous permafrost hundreds of meters thick (Osterkamp and Payne, 1981). Unconsolidated, surficial deposits are frozen and often include massive ground ice (Farquharson et al., 2016). Active layers, the near-surface layers of the ground that thaw each summer, are presently 20- to 50-cm thick (Osterkamp and Payne, 1981).

Despite the semi-arid climate, many soils on the North Slope remain saturated most of the year due to the shallow permafrost table that impedes drainage. As a result of the cold soils, perched water tables, and frequent cryoturbation, cycling of soil carbon is slow and can take millennia (Ping et al., 2015). As a result, thick soil organic horizons have accumulated during post-glacial times and now play important roles in ecosystem function (Baughman et al., 2015). In addition to insulating the permafrost from summer thaw, these peaty soils and the vegetation they support have stabilized extensive aeolian deposits dating to the last ice age (Carter, 1981; Galloway and Carter, 1993).

2.2. Regional Quaternary geology

Much of the North Slope escaped glaciation (Fig. 1) because of reduced precipitation during the coldest times of the ice ages (Hopkins, 1982). As a result of this lengthy glacier-free history, surficial deposits on the North Slope consist of a complex mosaic of fluvial, aeolian, colluvial, and marine deposits (Fig. 1) (Dinter et al., 1990; Farquharson et al., 2016). Repeated marine transgressions dating as far back as the Pliocene left on- and off-lapping deposits of marine silt and sand across the Arctic Coastal Plain (Dinter et al., 1990).

2.3. Fluvial processes

Alluvial deposits in valleys draining the Brooks Range are dominated by glacial outwash. In contrast, the Titaluk and Ikpikpuk Rivers did not receive glacial runoff during the ice age because meltwater and outwash from the Brooks Range were diverted to

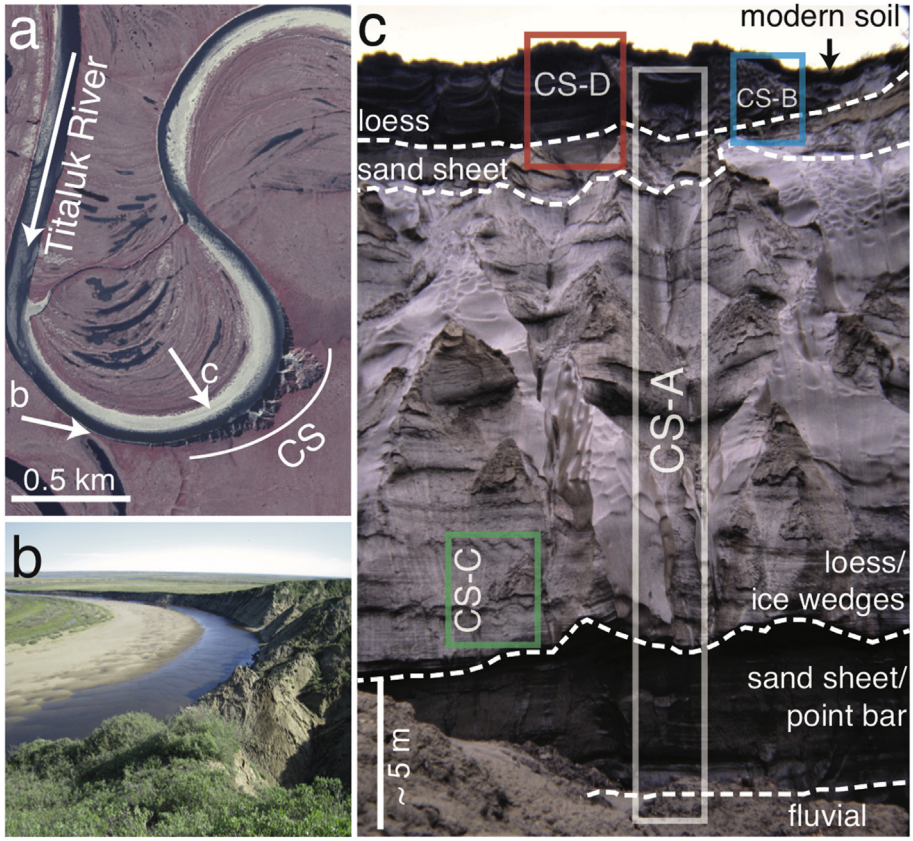

Fig. 2. a) The Carter Section is a cutbank of the meandering Titaluk River. Arrows show perspectives in photographs b and c. b) Oblique view of the Carter Section in 2012. c) Carter Section in 1994 showing syngenetic ice wedges penetrating the lower loess unit with sand sheet deposits above and below it. Boxes delineate the relative positions of the individual sections described and sampled in this study. Bottom of photo is around 17 m above river level.

the Beaufort Sea by the east-west trending Colville River (Fig. 1). The Titaluk ("Sheefish River" in Inupiaq) and Ikpikpuk ("Big Sand Bluff River") are low-gradient, meandering streams carrying sandy bedloads derived from local bedrock (Mann et al., 2010). Because of the long winters and rarity of heavy summer rains, these rivers experience nival flow regimes, meaning the break-up flood in early June is the only major flood in the course of a year. Today, the channels of both these rivers are deeply (10–50 m) incised within terraces dating to Late Glacial and early Holocene times (15–8 ka) (Mann et al., 2010). Floodplain aggradation and incision in the Titaluk valley have been controlled by changing rates of sediment input from adjacent hillslopes, which in turn have been controlled by interactions between active-layer thickness and periglacial processes (Mann et al., 2010). Base level in the lower reaches of the Titaluk River is potentially affected by the ISS, which has episodically overrun the lower valley (Dinter et al., 1990; Mann et al., 2010).

2.4. Aeolian processes

Near their confluence, the Ikpikpuk and Titaluk Rivers enter the stabilized ISS (Carter, 1981) (Fig. 1). The ISS consists of a central zone of linear dunes with vertical relief ranging up to 30 m and oriented northeast to southwest (Carter, 1981) (Fig. 3). Superimposed on these large linear dunes are scattered parabolic dunes, most of which are now stabilized. The central dune field is surrounded by an irregular aureole of aeolian sand-sheet deposits, and, along the hill front to the south and west, by a 10–30 km wide loess belt (Carter, 1988; Carter and Galloway, 1993). A similar sequence of sand dunes, sand sheets, and loess belt surround other high latitude dune fields; for instance, the Great Kobuk Dunes in northwestern Alaska (Mann et al., 2002a). Sand sheet and loess belts are fed by sediment derived from the central dune fields (Carter, 1988; Carter and Galloway, 1993; Mann et al., 2002a).

A northeast-southwest bimodal wind regime exists on the North Slope today, although the strongest winds are from the northeast in all seasons (Fig. 3). The northeast-southwest orientations of both the Pleistocene-aged linear dunes and the Holocene-aged parabolic dunes indicate a similar wind regime has existed since the Pleistocene (Carter, 1981; Hopkins, 1982).

Although the chronology remains uncertain, the large linear dunes in the ISS are thought to have last been active during the Late Pleistocene (Carter, 1981, Carter and Galloway, 1993). The parabolic dunes on top of them record Holocene-aged blowouts (Galloway and Carter, 1993). Occasional active blowouts occur today in recently drained thaw lake basins and along stream cutbanks that are oriented perpendicular to the predominant wind directions.

Other source areas for aeolian sediment besides the ISS exist along the Ikpikpuk and Titaluk Rivers, but these are small in area and involve relatively minor amounts of sediment. Where the Ikpikpuk and Titaluk Rivers cross the former sand sea, wide expanses of sandy point bars are exposed to reworking by the wind, resulting in the development of localized sand sheets and coppice dunes (Figs. 2 and 4).

It is unlikely the Ikpikpuk and Titaluk Rivers posed major barriers to the southward movement of aeolian sand at times when the ISS was active. Today, the floodplains of these rivers cut wide swathes across the stabilized ISS (Fig. 1), but these valleys have

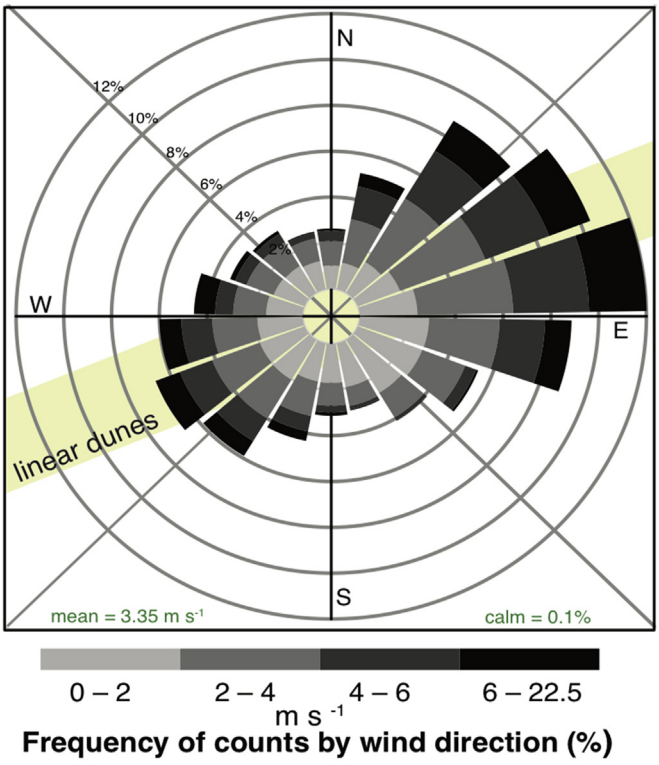

Fig. 3. a) Wind direction and speed between 2004 and 2016 based on hourly wind data collected 14.5 km southeast of the Carter Section at a height of 3 m above ground (https://pubs.usgs.gov/ds/0977/Inigok/Inigok.html). Yellow shading denotes the orientation of linear dunes in the ISS (Carter, 1981). (For interpretation of the references to colour in this figure legend, the reader is referred to the Web version of this article.)

been incised during post-glacial times (Mann et al., 2010). Today in summer, the Titaluk and Ikpikpuk Rivers are often reduced to pools connected by shallow riffles. During the driest periods of the ice age, both these rivers may have been ephemeral streams or disappeared altogether.

3. Methods

3.1. Field sampling

We described and sampled stratigraphic exposures at the Carter Section during summers between 2003 and 2014 (Figs. 2, 4–7). We used hand tools to clear slumped and thawed material and to prepare near-vertical faces of frozen sediment (Figs. 2, 4–7). A thin layer of sediment was allowed to thaw before it was described and sampled. Vertical heights were estimated using measuring tape, hand levels, and a surveying level. We described particle sizes and sedimentary structures in the field using standard methods and terminologies (i.e., Reineck and Singh, 2012). We used sediment and bedforms preserved in modern fluvial and aeolian deposits to help interpret ancient depositional environments exposed in the section (Figs. 2, 4–7). Periglacial features including sand wedges, ice-wedge pseudomorphs, and ice wedges were identified in accordance with Washburn (1980), Murton (1996, 2001), Murton and Bateman (2007), and French (2013).

3.2. Radiocarbon dating stratigraphic sequences

Age control comes from radiocarbon (^{14}C) dates on vascular plants rooted in growth positions (Figs. 6–7). We also dated animal feces and vole nests that were intercalated with silt and sand layers (Fig. 7). We used the ^{14}C ages of plants rooted at the uppermost levels of overbank deposits to constrain the timing of floodplain aggradation. We avoided dating detrital plant fragments because of the likelihood of their long-term preservation in permafrost (Gaglioti et al., 2014). Samples were prepared for ^{14}C dating using acid-base-acid rinses (Brock et al., 2010). Prepared material was then ^{14}C-dated using an accelerator mass spectrometer at the Beta Analytic Laboratory in Miami, Florida. Individual ^{14}C dates were calibrated using the IntCal13 curve (Reimer et al., 2013). A cubic spline age-depth curve using sampling depths and calibrated ages of ^{14}C dates with their 95% confidence limits was modeled for the Carter Section A (CS-A) and Carter Section D (CS-D) using the 'Clam' package (Classical, non-Bayesian age-depth modeling) in Rstudio software (Version 0.99.486) (Blaauw, 2010). This model allows estimates of the ages of sedimentary features and transitions lying between ^{14}C-dated samples. We also use this age-depth curve to estimate sedimentation rates, and, combined with dry bulk density and carbon content (described below), to estimate mass- and carbon-accumulation rates.

3.3. Geochemistry and particle size analysis

Sediment at different heights in the section was sampled using a volumetric sampler (747 cm^3) and then analyzed for bulk density, percent organic and inorganic carbon (% OC and % IC, respectively), and nitrogen (% N), as well as for plant macrofossils, and particle size. Samples were collected every 0.5–1.5 m in height from the CS-A and CS-B sections, and every 0.1–0.2 m in height from the CS-C and CS-D sections. Dry bulk density was estimated by drying a known volume of sediment (747 cm^3) in an oven at 70 °C for 48 h and then weighing it.

To estimate the abundance of vegetation growing at the Carter Section at various times in the past, we analyzed root biomass along with % OC and % N content in soils developing on modern point bars differing in their vegetation cover (Fig. 8). We visually estimated percent cover (mostly of grasses, Poaceae) in 1-m^2 areas (Fig. 8) (Westhoff and Van Der Maarel, 1978). Then we took three to five volumetric sediment samples (747 cm^3 each) from a depth of 10 cm at the center of each plot and analyzed them for % OC and % N (see below). Dry coarse organic biomass - mainly rootlets – was weighed and expressed as mass/volume after sieving through a 500-μm screen.

We assessed the relative abundance and nature of the ancient vegetation cover by sieving ~500 cm^3 of sediment from each sampled level through a 500-μm mesh screen and then describing the relative amount and type of plant remains. We qualitatively rated the amount of plant remains in each sample as *rare, uncommon, common,* or *abundant* based on the area of a gridded petri dish that the plant remains covered while suspended in water. The presence of wood was taken to indicate that woody shrubs were present. Percent OC provided an additional proxy for vegetation cover.

We analyzed % OC and % N after removing carbonates by soaking 1 cm^3 of dry sediment in a 10% HCl mixture overnight. Samples were then centrifuged, decanted, and rinsed with de-ionized water until reaching a pH of 5.5. Acidified and untreated sediment samples were then freeze-dried and weighed into tin capsules. These samples were then analyzed for carbon and nitrogen content on the LECO TruSpec CN analyzer by analyzing the products of sample combustion at 950 °C for carbon dioxide (CO_2) using an infrared CO_2 detector, and for nitrogen using a thermal conductivity cell. We estimated analytical precision as the standard deviation of values based on two replicates of the National Institute of Standards and Technology Buffalo River Sediment standards per 40 samples (total

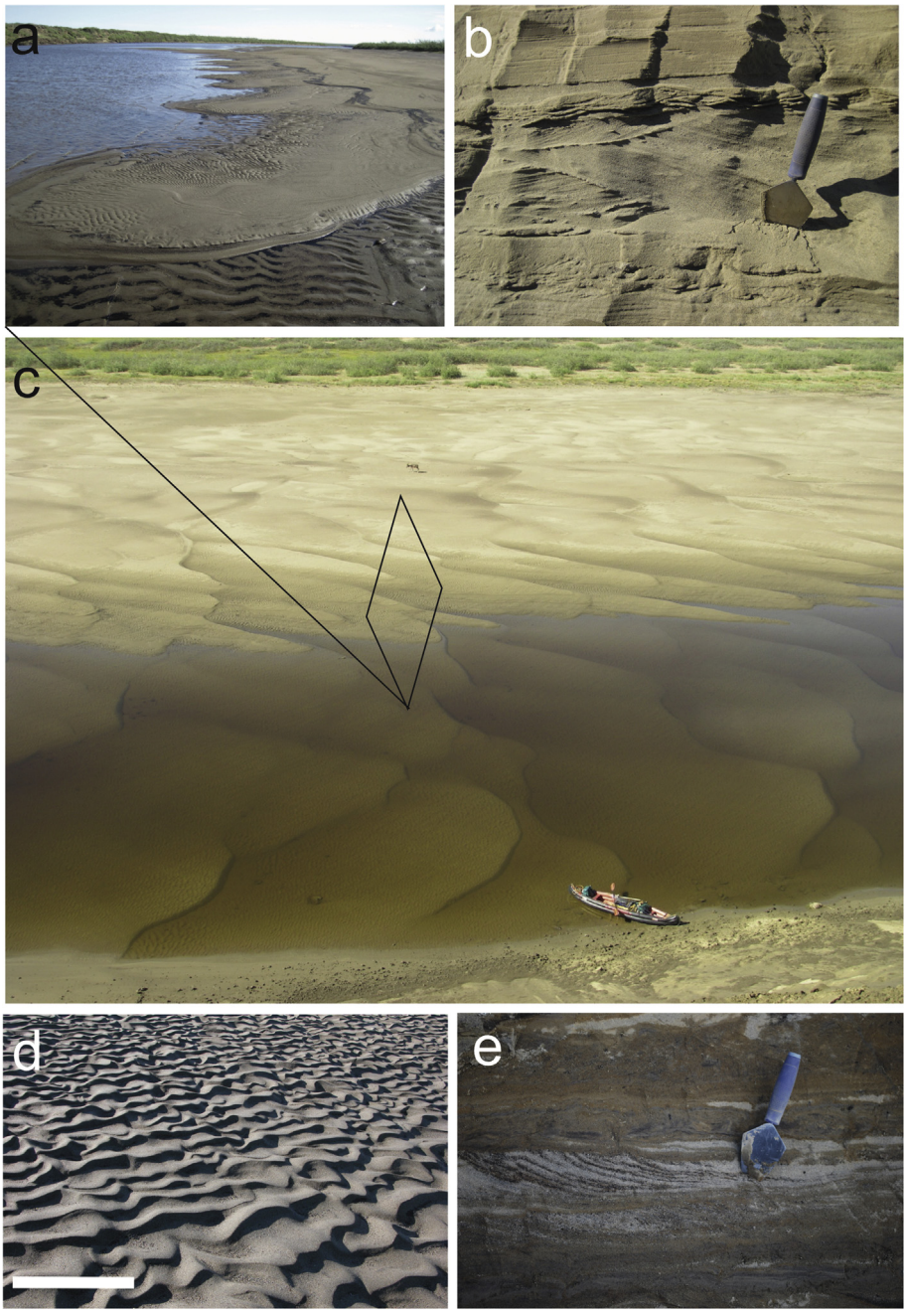

Fig. 4. Fluvial deposits along the Titaluk River today and in the Carter Section. a) View upstream showing fluvial dunes overriding current ripples formed at lower flow. b) Cross-trough beds in coarse and medium sand interbedded with plane beds - typical of a variable flow regime in lower, fluvial unit ofCarter Section A. c) Fluvial dunes formed during the spring flood. River flows to the right. Canoe and caribou on point bar for scale. Oblique square shows the orientation of Fig 4a. d) Linguoid ripples on point bar. Scale bar is 20 cm e) Planar laminae of fine sand and organic silt interlayered with trough crossbeds of medium and coarse sand in lower fluvial unit of Carter Section-A.

standard deviation for all standards were <0.011% N and <0.02% C). Percent OC was measured on acidified sediment, while % IC was calculated by subtracting % OC from the percent total carbon measured in untreated sediment from the same sampled level. We estimated organic carbon to nitrogen ratios (C:N) of sedimentary organic matter by dividing % OC by percent total N.

The particle sizes of 2–5 samples from each non-fluvial, sedimentary unit within the section were analyzed using a Horiba laser diffraction Grain Size Analyzer LA-920 at the National Lacustrine Core Facility (LacCore) at the University of Minnesota using their standard operating procedures (http://lrc.geo.umn.edu/laccore/assets/pdf/sops/Horiba Grain Size Analysis SOP, 2010.pdf). First, organic matter and carbonate were removed from sediment samples using wet chemical digestion. Pre-treated samples were then analyzed for particle size using laser diffraction (Jiilavenkatesa et al., 2001). Particle size data was analyzed using the Gradistat extension of Microsoft Excel (Microsoft Office OSX 2011) (Blott and Pye, 2001). To compare the particle size fraction of different sedimentary units, we calculated percent clay, silt, and sand using the particle-size classification of Folk (1966).

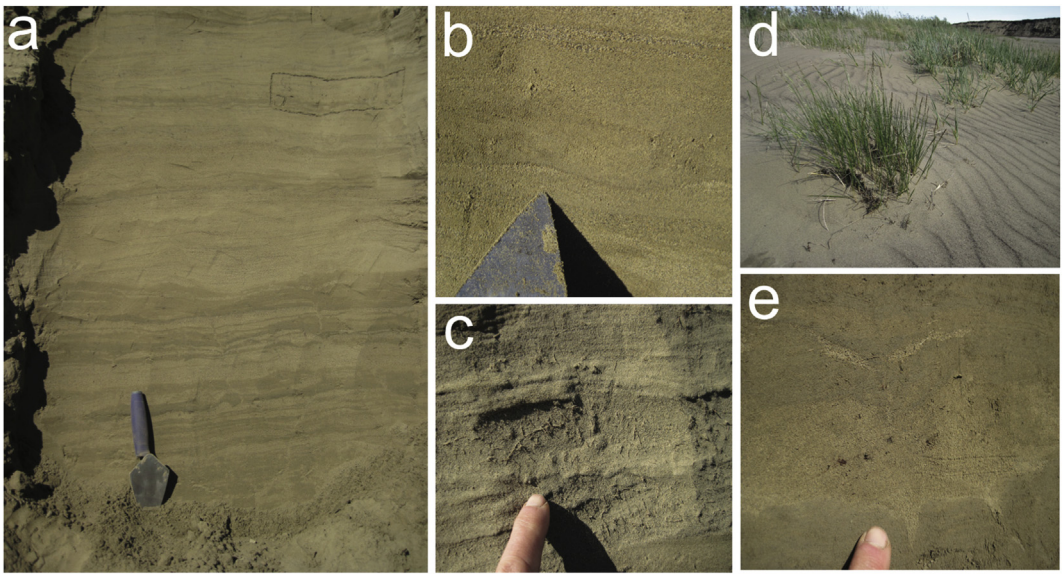

Fig. 5. Sand-sheet deposits on the North Slope today and in the Carter Section. a) Wavy, subhorizontal beds and laminae of fine and medium sand. Trowel for scale. b) Close-up of stranded coarse-grained wind ripple crest. c) Close-up of graminoid rootlets in sand-sheet deposit. d). Grassy sand sheet on a Titaluk River point bar today. Note the coarse-grained crests of wind ripples interacting with vegetation. e). Former location of a rooted plant in Carter Section-A. Wind-scour created a depression around the former stem, and root channels disrupted the underlying sand strata.

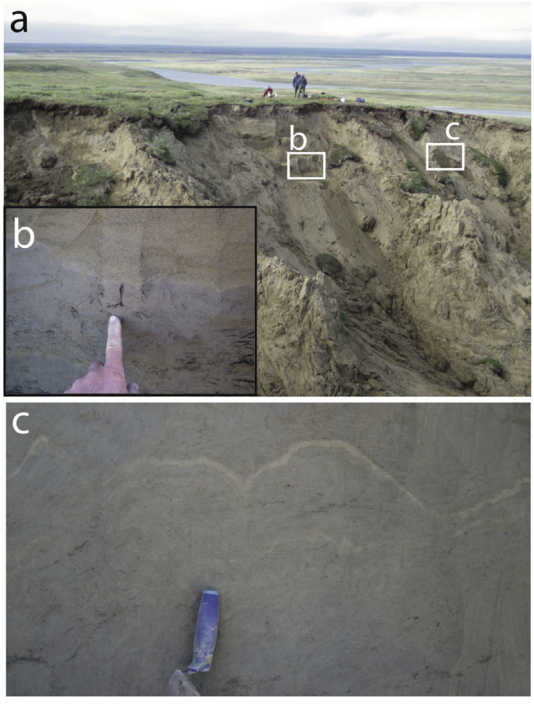

Fig. 6. a) Upper portion of the main loess unit in Carter Section A (CS-A). White boxes show locations of photographs b and c. b) The main loess – upper sand sheet transition. Note grain size changes and the massive structure of the loess. Finger points to a rooted plant truncated by the erosive contact between the two units. c) Paleo-surfaces are occasionally preserved in the main loess unit by thin layers of coarser material, in this case fine sand. Trowel for scale.

4. Results

4.1. Sedimentary facies: ancient and modern

Today fluvial deposits of the Titaluk River are dominated by high-angle cross-bedding deposited as fluvial dunes and by climbing ripple cross-laminae deposited within scour hollows and channel thalwegs as the break-up flood recedes (Fig. 4). As on similar Arctic floodplains (Ashley and Hamilton, 1993), other sedimentary features include the vertical juxtaposition of coarse- and fine-grained sediment indicative of rapid changes in current velocity. Lenses and laminae of re-worked organic material including comminuted peat, leaves, twigs, and coal fragments are common, particularly in association with climbing-ripples (Fig. 4). While rooted plants are absent from channel deposits, willow shrubs in growth position occur commonly in modern overbank deposits, which consist of subhorizontal beds and laminae of fine sand and silt that frequently contain laminae and lenses of detrital organics (Fig. 4). As the summer progresses and the river level drops, aeolian processes re-work the exposed surfaces of point bars, leading to complex mixtures of sand-sheet and fluvial sedimentary features (Figs. 4 and 5).

Aeolian sand-sheet deposits consist of horizontal to undulating beds and laminae of predominately fine and medium sand that lack the high-angle slip-face deposits of sand dunes (Fig. 5) (Lea and Waythomas, 1990; Mann et al., 2002a; Bateman and Murton, 2006). Based on 12 particle-size samples, sand-sheet deposits have mean (standard deviation) compositions of sand 66% (18%), silt 29% (17%), and clay 5% (1%). Individual layers and laminae of sand pinch and swell in thickness as a result of interactions between wind-ripple crests and scattered vegetation (Fig. 5). Unlike the fluvial deposits of the modern Titaluk River, sand sheets rarely contain organic layers or high-angle cross-laminae, and only limited variation occurs in particle size (Koster and Dijkmans, 1988; Lea, 1990; Neuman, 1993). Other diagnostic features include the presence of lags of coarse sand grains and isolated, convex-up, inversely-graded ripple crests that mark former truncation surfaces (Fig. 5). Partly decayed, herbaceous plants with roots extending through multiple strata occur in modern and ancient sand-sheet deposits (Figs. 5 and 7). Evidence for sand dunes is rare in the Carter Section. Where it does occur, it consists of truncated foreset beds of well-sorted, medium sand deposited in medium-scale sets of high-angle cross strata showing evidence for a

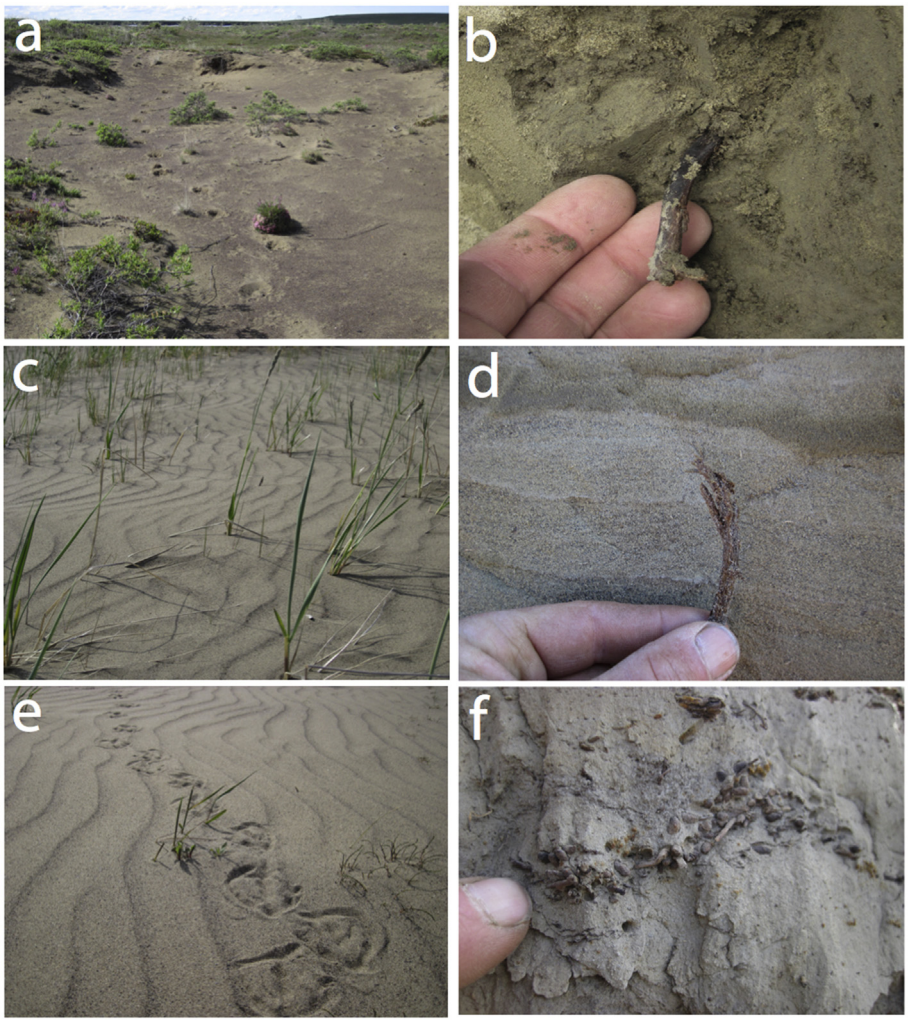

Fig. 7. Modern analogues (left column) for ^{14}C-dated samples in the Carter Section (right column). a) Willow shrubs in sand sheet. b) Shrub stem in growth position in mid-Wisconsin soil in the CS-C section. c) Rye grass (*Elymus* spp.) in sand sheet along the Titaluk River. d) Graminoid stem in a sand-sheet unit in CS-A. e) Sand sheets are biologically active. Goose tracks and raindrop impacts on modern sand sheet. f) Ancient vole latrine in the upper CS-A sand sheet.

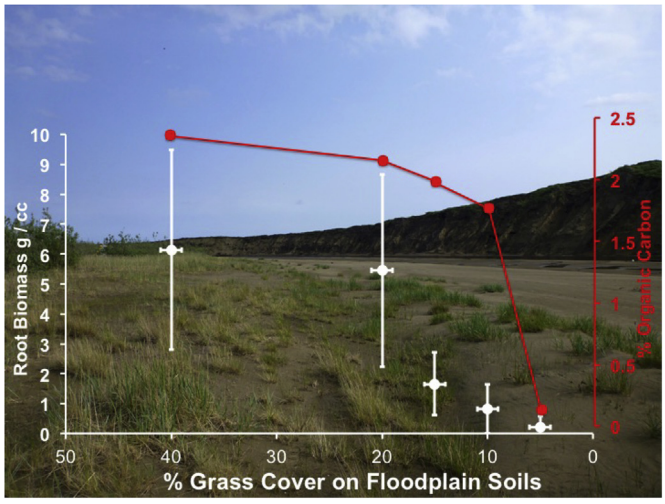

Fig. 8. Organic carbon (OC) and root biomass in sand-sheet soils developing on modern point bars of the Titaluk River that vary in vegetation cover (% grass cover). All biomass and % OC samples are from a depth of 10 cm.

mixture of grainfall, slump, and grainflow stratification (Lea, 1990; Bateman and Murton, 2006; Reineck and Singh, 2012).

Loess deposits in the Carter section vary from sand-rich to sand-poor in texture (Fig. 6). As at other sites in Alaska (Muhs et al., 2003a; Jensen et al., 2016), primary loess is deposited as air-fall dust and consists mainly of silt with minor components of sand and clay (Murton et al., 2015). In outcrop, primary silt-rich loess is typically homogenous and unstratified, although faint horizontal laminae are usually present (Muhs et al., 2003b) (Fig. 6). Secondary loess deposits are defined by increased stratification and small-scale cut-and-fill structures indicating shallow reworking of air-fall deposits by wind and in some cases by the overland flow of water (Murton et al., 2015). Rootlets are ubiquitous in silt-rich loess in the Carter section (Fig. 5), occasional non-woody stems and root systems are preserved in their growth position, and mammal feces, bones, and rodent nests are occasionally encountered (Figs. 6 and 7). Faint, horizontal bands of oxidation record pedogenesis occurring as the sediment accumulated. Based on 12 particle size samples, deposits that we identified as silt-rich loess had a mean (and standard deviation) of sand 28% (21%), silt 66% (20%), and clay 6% (1%).

4.2. Calibrating paleo-plant cover using modern point-bar soils

On modern point bars of the Titaluk River, areas with more dense vegetation cover had higher % OC and more abundant coarse, organic biomass (Fig. 8). Areas with <5% grass cover had ~0.3% OC and a mean of ~0.3 g coarse organics/cm^3 coarse organics, whereas areas with 10–25% grass cover had 1.5–2.5% OC and 1–5 g coarse organics/cm^3 coarse organics. Areas on the modern point bars with the highest non-woody plant cover (45%) had ~2.4% OC and ~6 g coarse organics/cm^3.

4.3. Carter Section stratigraphy and depositional setting

4.3.1. Carter Section A

4.3.1.1. Basal fluvial unit. The ^{14}C-dated portion of Carter Section A (CS-A) begins 21.8 m above the level of the Titaluk River as observed on 9 July 2011 and extends to the bluff top, 48.5 m above river level (Fig. 9). The described section begins at the boundary between the underlying fluvial unit and overlying aeolian one. In what follows, locations in the section are described according to depth below the top of the section. The water-lain deposit below the 26.7-m level consists mainly of channel scours, trough cross-beds, and fluvial climbing ripples in medium to coarse sand (Figs. 4 and 9), which is consistent with deposition by a meandering channel of the paleo-Titaluk River (Fig. 4). The orientation of cross-beds indicates that the paleo-flow direction of the river was towards 290° and 270° (Fig. 9).

4.3.1.2. The lower sand-sheet unit. Sand-sheet deposits begin 26.7 m below the bluff top in CS-A (Fig. 9). An herbaceous stem in growth position immediately above the fluvial-aeolian contact dates to 36.6–37.4 ka (date A-16 referred to in figures and Supplemental Table 1). Above this contact, sand-sheet deposits extend upwards to the 20.5-m level. Occasional low-angle cross-beds of medium sand indicate the presence of low dunes, < 1 m in height deposited by wind blowing towards 260° (Fig. 9). In the uppermost meter of this unit, dune foresets developed in medium and coarse sand record wind blowing towards 230°. Overall, this aeolian sand unit possesses the highest percent-sand content in the entire section (~90%) (Supplemental Fig. 1). The presence of scattered root clumps and stoloniferous stems indicate scattered graminoids and herbaceous plants were present when this unit accumulated (i.e., Fig. 7c); however, the sparse plant remains found in sieved samples and the low % OC (<0.5%) indicate this plant cover was sparse. Even though the overall organic carbon is low (Fig. 10), a period of high carbon accumulation (>15 g C/m/yr) occurred ca. 36 ka, perhaps when a rapidly accumulating sand layer buried plant material before it had time to either blow away or decompose.

In summary, the lowest aeolian unit in CS-A accumulated between ca. 34.5 ka and 37.4 ka and records low coppice dunes and sand sheets supporting scattered, herbaceous (non-woody) vegetation (Fig. 10). The site was probably an abandoned point bar of the Titaluk River.

4.3.1.3. The main loess unit. In CS-A, the transition from sand-sheet and dune deposits to silt-rich loess occurs between the 20.0 and 19.7 m depths. This lower loess unit extends upwards to the 5.0-m level and is composed mainly of silt with 10–20% fine sand (Fig. 9, Supplemental Fig. 1). ^{14}C dates on *in situ,* non-woody plants (A-3, and A-6 through A-12) and buried animal feces (*cf.* vole or lemming, Microtinae (A-4) and *cf.* caribou, *Rangifer tarandus* (A-5)) record deposition between ca. 18.4 and 34.5 ka (Figs. 9 and 10). Mass accumulation rates (MARs) in this loess unit varied, but were similar or slightly higher than MARs in the upper and lower sand-

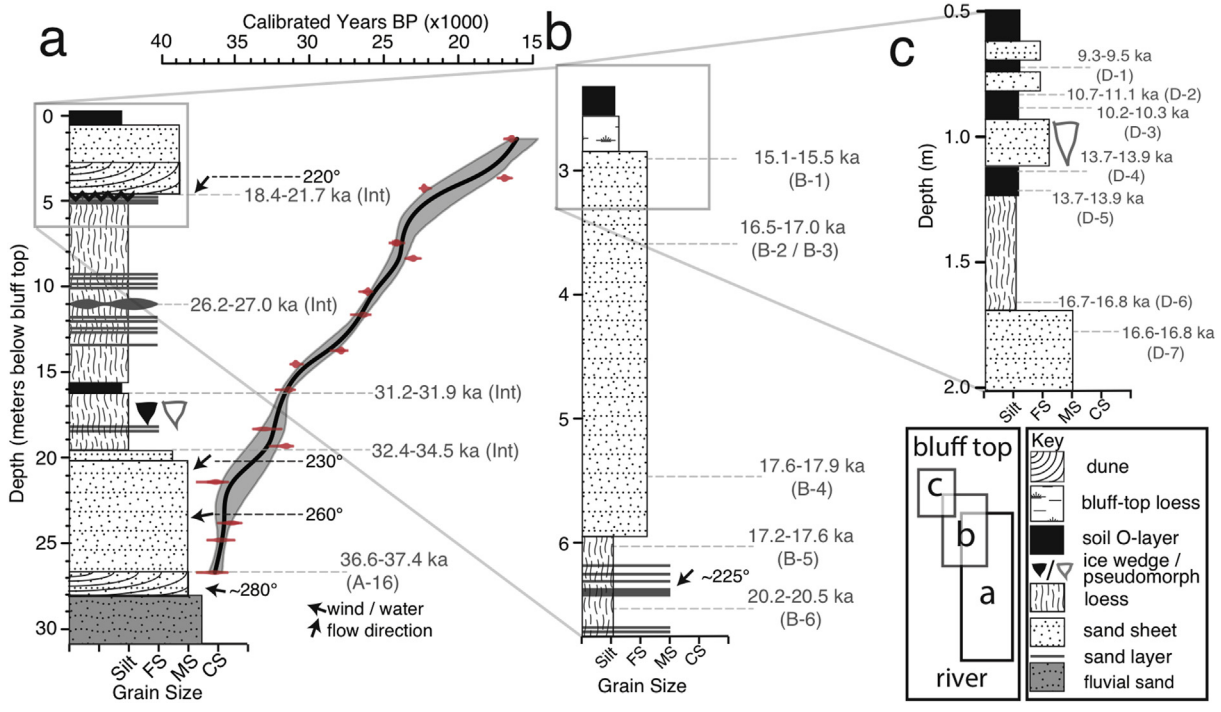

Fig. 9. Stratigraphy and ^{14}C ages in the Carter Section (CS). a) CS-A with positions of ^{14}C-dated plant macrofossils (red), smoothing spline age-depth modeling interpolation (black line) and 95% range of interpolation (gray shading). Age estimates for sedimentary transitions labeled in gray. Arrows indicate flow directions inferred from bedforms. Grain-size abbreviations: fine sand (FS), medium sand (MS), and coarse sand (CS). Horizontal bars in stratigraphy column depict sandy laminations and beds. Undulating lines show locations of former soil surfaces. Saw teeth indicate erosive contacts at unit boundaries. b) CS-B spans the uppermost 7 m of CS-A. c) CS-D spans the uppermost 3.5 m of CS-B. (For interpretation of the references to colour in this figure legend, the reader is referred to the Web version of this article.)

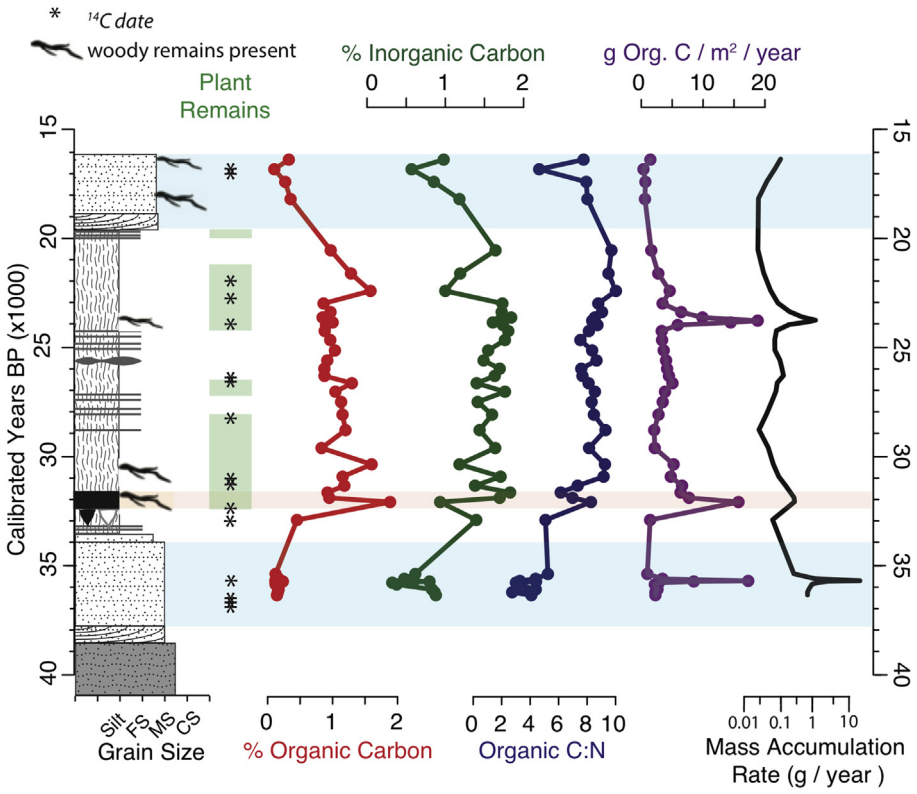

Fig. 10. Stratigraphy, sediment accumulation rates, and geochemistry plotted on the age-depth model of CS-A. Pink horizontal shading marks the organic-rich, mid-Wisconsin paleosol complex. Blue horizontal shading marks the sand sheet units. Sedimentary units and grain sizes are the same as in Fig. 9. Green shading shows when plant remains are abundant. Location of ^{14}C ages noted with asterisks. (For interpretation of the references to colour in this figure legend, the reader is referred to the Web version of this article.)

sheet units (Fig. 10).

A horizon of epigenetic ice wedges occurs at the 17–19-m level in the lower part of the main loess unit in CS-A (Fig. 9). These small wedges are 30–75 cm wide at their top surfaces and extend 1–2 m vertically. We interpret them as being epigenetic rather than syngenetic because they are relatively small, vertically discontinuous, and taper continuously from top to bottom unlike syngenetic wedges (French, 2013). Their planar, upper surfaces coincide with buried soils whose undulating upper surfaces are consistent with deformation during ice-wedge growth. This subunit was best exposed in the CS-C section and is described in more detail in Section 4.3.3.

In terms of depositional environment, the main loess unit in CS-A records airfall loess deposited on a surface supporting vegetation denser than was present during the periods of sand-sheet deposition that preceded and followed it. Percent OC (1.0–1.5%), % IC (1.5–2.0%), and C:N (>5) are higher in this loess unit than in either sand-sheet unit (Fig. 10). Wet sieving of bulk samples of the loess yielded more abundant plant remains (mainly rootlets) than the sand-sheet units, suggesting denser vegetation (Figs. 8 and 10). As described in more detail in Section 4.3.3, vegetation cover was probably continuous at the time the buried soil formed in the lower part of the loess unit.

4.3.1.4. The upper sand sheet. At the 5-m depth in CS-A, loess abruptly switches back to sand sheet across an erosive contact that cross-cuts rooted plants and truncates sub-horizontal bedding in the underlying loess (Figs. 6 and 9). This transition occurred sometime between 17.0 and 21.7 ka based on limiting ^{14}C ages of *in situ* plants above (A-2) and below (A-3) the transition. In the lower portion of the upper sand-sheet unit, a 1-m-thick zone of foresets records a low dune migrating towards 220° (Fig. 9). Sand-sheet deposits conformably overlie these dune foresets and extend upwards to 0.55 cm below the ground surface. This upper sand-sheet unit contains more numerous truncation surfaces and more irregular (wavy) bedding than the lower sand-sheet unit (Section 4.3.1.2). Mass-accumulation rates are lower than anywhere else in the section (Fig. 10), which, along with the cut-and-fill features, suggests this unit was repeatedly affected by deflation. Plant remains in the sieved fraction and % OC are low (<0.5%) (Fig. 10), suggesting a sparsely vegetated surface (Fig. 8). Although C:N tends to be higher than in the lower sand-sheet unit (Fig. 10), the plants that were present were probably widely spaced. The upper boundary of this sand unit occurs at an abrupt, possibly erosive contact with an overlying layer of loess underlying the modern soil. A plant in growth position 75 cm below this sand to silt transition dates to 16.7–16.9 ka (A-1).

In summary, the CS-A section records two alternations of sand-sheet and loess deposition (Figs. 9 and 10). The first sand-sheet to loess transition occurred ca. 33 ka. The subsequent period of loess deposition was replaced by sand-sheet deposition sometime between 17 and 21.7 ka that ended sometime shortly after ca. 16.8 ka. Plant cover exceeded 10% during deposition of the main loess unit but was significantly lower' when the overlying sand sheet was deposited.

4.3.2. Carter Section B

4.3.2.1. The loess-upper sand sheet transition. Carter Section B (CS-B) is located 300 m downstream (northeast) of CS-A where the bluff top is 4.9 m higher than the top of CS-A. The CS-B section extends from 7 m below the bluff top upwards to the modern vegetation mat (Figs. 2 and 9). We investigated this section in order to study in

more detail the post-20 ka portion of the stratigraphy.

The described section begins 1.2 m below the main loess-upper sand sheet contact, which is present as an erosional unconformity in the CS-A section (Fig. 9). In the CS-B section, several rooted plants span the loess-sand contact, and strata in the loess unit are not crosscut by the contact (Fig. 9), suggesting little or no erosion occurred during the loess to sand sheet transition. Herbaceous plants in growth position date to 17.2–17.6 ka (B-5) directly below and 17.6–17.9 ka (B-4) directly above the loess-sand sheet contact (Fig. 9). Isolated wind-ripples in the lower loess unit of CS-B record wind blowing towards 225°.

4.3.2.2. The upper sand sheet. At depths between 5.86 and 2.46 m, medium and fine sand contains small-scale cut and fill structures, convex-up ripple crests, and abundant rootlets (Figs. 5 and 9). Across a 10-cm transition zone centered at a depth of 2.46 m, sand-sheet deposits fine upwards into silty, very fine sand and then into massive, silt-rich loess. An *in situ* herbaceous plant 10 cm below this transition at the top of the upper sand-sheet unit dates to 15.1–15.5 ka (B-1). Organic content is low in the sand-sheet deposit, and the total percent sand is less than in the lower sand sheet unit of CS-A (Supplemental Figure 1). No woody macrofossils occur in the upper sand-sheet unit of CS-B. Overall, herbaceous plant remains were rare in the sieved fraction, and % OC was low (<0.5%). The uppermost 2.46 m of CS-B consists of alternating layers of loess and peat representing intermittent soil development and deposition of silt and sand that is revealed in more detail in CS-D (Section 4.3.4).

In summary, the CS-B section constrains more closely the transition from the main loess unit to the upper sand sheet as having occurred between 17.6 and 17.9 ka (Fig. 9). The subsequent transition from sand sheet back to loess is also more precisely constrained as occurring shortly after 15.1–15.5 ka. Sparse, widely-spaced vegetation with <5% cover on sand-sheet deposits is similar to that inferred in this same unit in CS-A.

4.3.3. Carter Section C

To investigate in more detail the prominent buried soil occurring at 17–18 m depth in CS-A (Figs. 2, 9 and 10), we excavated another exposure of the same soil in the CS-C section located ~240 m downstream (Figs. 2 and 11). When we first visited it in 2003, CS-C was a *baydzherakh* whose sides revealed the lower portion of the main loess unit described in CS-A. The CS-C section begins in the lower sand-sheet unit, 40 cm below the contact between the lower sand sheet unit and the main loess (Fig. 2). The sand sheet to loess transition occurs here over a 20–30 cm zone of interbedded sand-sheet and loess deposits.

Two meters above the loess to sand sheet transition in CS-C, a 30-cm-thick layer of organic-rich, sandy silt contains abundant woody stems and roots (Soil 1, Fig. 11). The woody stems range in diameter from 1 to 3 cm, indicating the presence of large, upright shrubs, probably willows. These shrubs grew between 34.9 and 36.1 ka and 35.1–36.3 based on the calibrated ^{14}C-ages of a two woody stems in growth positions (C-5, C-6). Above this woody layer is a 50-75 cm-thick layer of massive, organic-poor silt-rich loess.

Continuing upward in CS-C, a ~15-cm-thick paleosol we refer to as the 'purple soil' lies above the massive loess layer, (Soil 2, Fig. 11). This soil has a cumulic structure with alternating bands of organic-rich silt and fine sandy silt. Woody stems, herbaceous plants, and rootlets are abundant. The soil is gleyed and contains a B/C horizon. A rodent latrine enclosed in loess ~10 cm below the purple soil yielded an age of 34.6–34.9 ka (C-4). Two shrubs in growth position from the same soil dated to 32.6–33.3 ka and 33.1–34.0 ka (C-1, C-3). The easternmost exposure of the purple soil was severely cryoturbated with alternating bands of organic layers and silt dipping

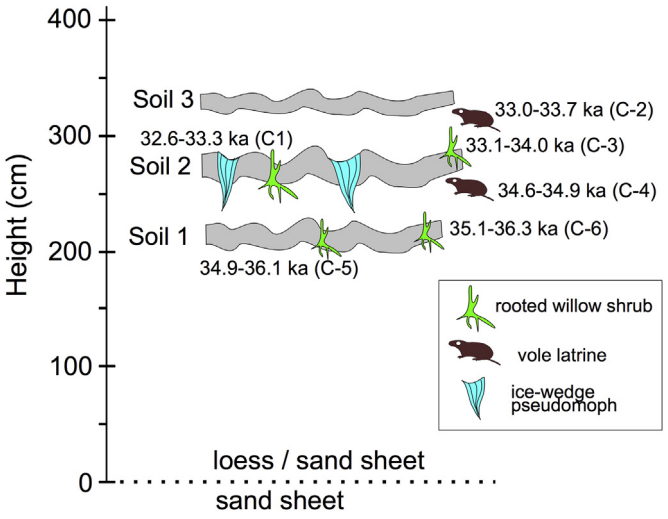

Fig. 11. Stratigraphy of the CS-C section showing multiple mid-Wisconsin buried soils and epigenetic ice-wedge pseudomorphs.

at angles up to 45°. Skull fragments of a young woolly mammoth were found in a slumped portion of this section. The cryoturbation features are probably the result of slumping into an epigenetic ice wedge pseudomorph coeval with development of the purple soil (distinguished using the same criteria described in Section 4.3.1.3). The purple soil is buried by loess above a non-erosional but abrupt boundary (Fig. 11).

Some 50 cm above the purple soil, a third soil horizon occurs (Soil 3, Fig. 11) that is 20–30 cm in thickness and is less oxidized and has a lower organic content than the purple soil, but nonetheless contains twigs, rooted plants, and rootlets. A rodent latrine ~10 cm below Soil 3 dates to 33.0–33.7 ka (C-2).

In summary, the CS-C section records repeated episodes of soil development and shrub growth between 32.6 and 36.3 ka in the lowermost part of the main loess unit. The presence of soils and epigenetic ice wedges imply loess deposition slowed significantly when they were developing. At the same time, vegetation cover increased, woody shrubs became abundant, and heightened net primary productivity allowed peat accumulation. The presence of epigenetic ice-wedge pseudomorphs indicates that, at least intermittently, active layers deepened enough to trigger thermokarst.

4.3.4. Carter Section D

Forty meters downstream of the CS-C, the CS-D section exposes sediment deposited during the Pleistocene-Holocene transition near the bluff top (Figs. 2, 9 and 12). The lowest part of this section begins in the upper sand-sheet unit described in CS-A and CS-B (Sections 4.3.1, 4.3.2).

4.3.4.1. Unit 1: the upper sand sheet. This unit is 31–60 cm thick and consists of laminae of fine to medium sand containing occasional, stranded, aeolian ripple crests and irregular truncation surfaces typical of a sparsely vegetated sand sheet (Figs. 9 and 12). No woody plant remains were found in this unit by wet sieving. Non-woody rootlets and plant remains are rare, and % OC is low (<0.5%) (Fig. 12). Two centimeters below the top of this sand-sheet unit, an *in situ* graminoid stem dated to 16.6–16.8 ka (D-7).

4.3.4.2. Unit 2: loess. A gradual (10-cm) transition between sand sheet and loess occurs above the sand-sheet unit. Above it lie 45–60 cm of silty, very fine sand with vague, horizontal bedding (Figs. 9 and 12). This sandy loess shows extensive oxidation in its

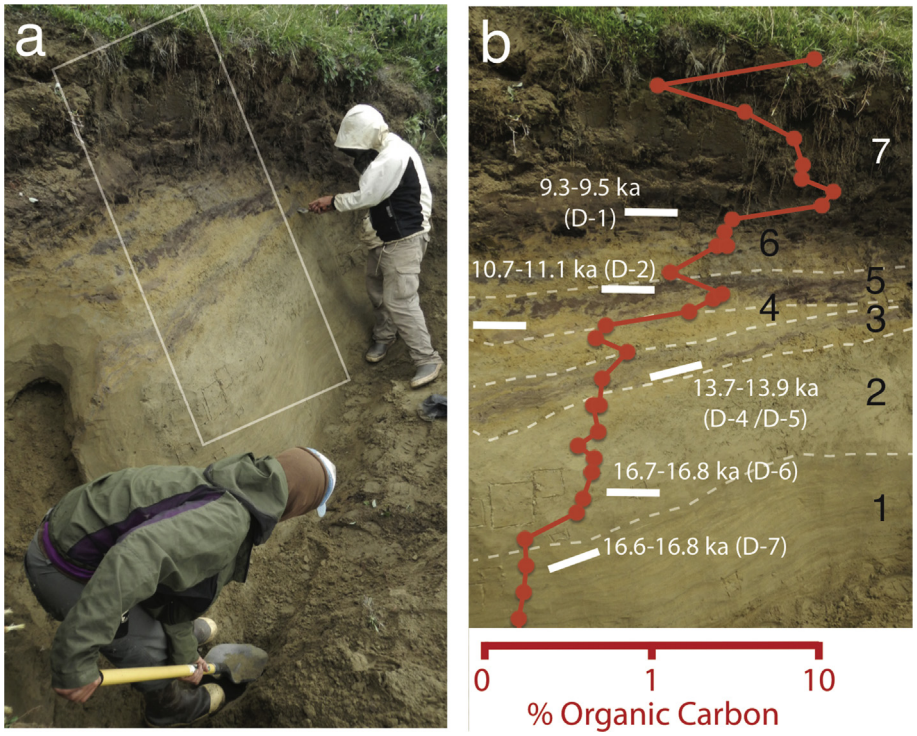

Fig. 12. a) The CS-D section showing the Pleistocene-Holocene transition. White box outlines the right-side panel. The hollow area visible to the left of the nearer laborer is an ice-wedge pseudomorph developed in Unit 4. b) Percent organic carbon and ^{14}C stratigraphy. *Unit 1:* sand sheet. *Unit 2:* loess. *Unit 3:* lower soil. *Unit 4:* sand sheet. *Unit 5:* middle soil. *Unit 6:* silty fine sand. Unit 7: bluff-top loess with multiple buried soils.

upper half. Non-woody plant stems are common, along with abundant rootlets. Percent OC is higher than in the underlying sand (0.5–0.75%). A non-woody plant in growth position within the transition between sand sheet and loess dated to 16.7–16.8 ka (D-6).

4.3.4.3. Unit 3: lower paleosol. Continuing upwards, the loess unit is overlain by an 8- to 12-cm-thick soil (Figs. 9 and 12). This buried soil contains an organic horizon containing well-decomposed organics overlying a B/C horizon. In places, the organic horizon is inter-bedded with silty sand. Percent OC is slightly elevated in this lower soil compared to the underlying loess (0.5–1.0%) (Fig. 12). A block of peat containing wood fragments from the lower 4 cm of this unit dated to 13.7–13.9 ka (D-4, D-5).

4.3.4.4. Unit 4: sand sheet. The Unit-3 soil is buried by another sand-sheet deposit (Figs. 9 and 12). This sandy unit has a sub-horizontal structure encompassing sand laminae and stringers of well-decomposed organic matter. Plant remains are non-woody, and sparse. *In situ* rootlets are uncommon, and % OC is lower than in the soils above and below this unit (0.5–0.75%) (Fig. 12). Based on the ^{14}C dates from plant remains in soils above and below, this sparsely vegetated sand sheet was deposited sometime between 10.7–11.1 ka and 13.7–13.9 ka (D-4, D-2), possibly during the Younger Dryas chronozone (11.7–12.8 ka). The pseudomorph of an epigenetic ice wedge (distinguished using the same criteria described in Section 4.3.1.3) lies within this unit and extends downwards into Unit 2. The fact that overlying bedding is undisturbed suggests this ice wedge formed between 11.1 and 13.7 ka and melted prior to 9.5 ka.

4.3.4.5. Unit 5: middle organic-rich paleosol. A 10- to 16-cm-thick, organic-rich paleosol overlies the Unit-4 sand sheet (Figs. 9 and 12). Its organic horizon is interlayered with gleyed, silty fine sand. Percent OC in this organic horizon increases with height to >1.0% (Fig. 12). A sample of well-decomposed organics from the lower 3 cm of this layer dated to 10.2–10.3 ka (D-3). Another sample of decomposed organics from the uppermost 3 cm of this unit dated to 10.7–11.1 ka (D-2). We interpret this unit as recording an episode of reduced aeolian deposition that permitted soil development, peat accumulation, and epigenetic ice wedge growth between 10.2 and 11.1 ka.

4.3.4.6. Unit 6: silty fine sand. Continuing upward in CS-D, a 5- to 15-cm-thick layer of silty oxidized, silty fine sand overlies the Unit 5 buried soil (Figs. 9 and 12). This unit contains several peat lenses similar to those occurring in Unit 5. Percent OC is low, and plant remains are uncommon. This unit records enhanced loess deposition burying the soil of Unit 5. Based on the limiting dates from the soils above and below this unit, this enhanced loess deposition occurred between 10.2–10.3 ka (D-1) and 9.3–9.5 ka (D-3) (Figs. 9 and 12).

4.3.4.7. Unit 7: modern soil. A bluff top-soil has accumulated since ca. 9.5 ka based on the lower-limiting age provided by D-1. This modern soil consists of a cumulic sequence of organic and B/C horizons. Percent organic carbon is high (>5.0%), and rootlets, woody material and plant remains are abundant. The relative thinness of this unit indicates aeolian deposition has been very slow since 9.5 ka.

In summary, the CS-D section provides a maximum-limiting estimate of 16.7–16.8 ka for the transition between sand-sheet and loess deposition. Alternations between sand sheets and soil formation occurred during the Pleistocene to Holocene transition. Sand sheets covered the site after 13.7–13.9 ka, and loess deposition accompanied by soil development resumed after 10.7–11.1 ka.

The last ca. 9.5 ka has seen slow accumulation of bluff-top loess and sand accompanying development of B horizons and peat deposition.

5. Discussion

5.1. Interpreting the aeolian record of the Carter Section

5.1.1. Sediment sources

The 27 m of aeolian sediment accumulated in CS-A over the last 37 ka was derived from two sources: the nearby floodplain of the Titaluk River and the ISS, whose core region of large-scale dunes at times lay just 10 km upwind and whose fringing sand sheets episodically crept over the site. The lower aeolian sand unit in the CS-A section was probably deposited by sand sheets and coppice dunes developing on a point bar of the ancient Titaluk River. We base this inference on the occurrence of numerous modern analogs for this same geomorphic setting, the presence of point-bar facies in fluvial deposits immediately below the Lower Sand Unit, and this sand sheet's relatively coarse grain size.

Currently, there is no evidence for fluvial inputs to the Carter Section at levels younger than ca. 37 ka, probably because the floodplain of the Titaluk River never again aggraded high enough to deposit fluvial sediment in the section. Both during the Bølling-Allerød and the early Holocene, the Titaluk and Ikpikpuk valleys aggraded rapidly, but they never came within 20–30 vertical meters of the top of the Carter Section (Mann et al., 2010).

Additional evidence that the Titaluk River was not an important sand sources for the upper units of the Carter Section comes from the "Russian Section" located 22 km upstream (downwind) (Fig. 1). This smaller cutbank exposure lies in the ISS' loess belt, and no upper sand-sheet unit occurs there; instead, the upper part of the section is composed entirely of loess deposited after ca. 24.5 ka (Supplemental Fig. 2). The lack of a sand-sheet facies in the upper Russian Section is consistent with the ISS rather than the Titaluk River being the predominant sediment source for both locations, with loess over-passing the Carter Section and being deposited around the Russian Section at times when the ISS was most active. If the upper sand sheet unit was derived from an aggrading river, the Russian Section would have likely recorded it, but this is not the case.

In a broader sense, it is futile to try to distinguish whether aeolian sediment came from a dune field or from the rivers flowing across it, simply because the two geomorphic systems are so intimately linked (Mann et al., 2002a; Wolfe, 2006). Today the Ikpikpuk and Titaluk Rivers are actively reworking dune deposits where they cross the stabilized ISS, and at the same time they are transporting sand derived from bedrock in their headwaters onto the coastal plain, where it will become part of a future ISS. The salient point here is that the ISS covered an area >7000 km^2 immediately upwind of the Carter Section (Fig. 1), and served as an enormous source area for aeolian sediment whenever it was active. With the exception of the lowest aeolian-sand unit, we interpret the sedimentology of the Carter Section to be primarily a record of changes in the extent and stability of the ISS.

5.1.2. Factors controlling the ISS

The activity of some dune fields is limited by sand supply, that of others by sediment availability (Kocurek and Lancaster, 1999). Sand supply is unlikely to have limited the activity of the ISS because cutbank exposures in the western part of the dune field reveal vertical thicknesses of aeolian sand >50 m thick (Mann et al., 2010), indicating a large quantity of sand was available for reactivation. This leaves sediment availability as the key factor controlling the extent and activity of the ISS.

The presence of permafrost endows Arctic dune fields with special attributes. On Alaska's North Slope, the thickness of the active layer is crucial for determining sand mobility. As Black (1951) observed:

> "But for permafrost, which impedes surface runoff and permits luxuriant vegetation to grow in spite of low precipitation, the coastal plain would be a desert with rapidly shifting sands."

It follows that warm summer temperatures can trigger dune activation by causing deeper thaw, enhanced soil drainage, and increased evapotranspiration - all of which cause increase physiological water stress for plants and so reduce vegetation cover (Carter and Galloway, 1993; Galloway and Carter, 1993). Similarly, Mann et al. (2002a) inferred that effective moisture, the amount of moisture available to supply runoff and soil moisture, controlled the Holocene activity of the Great Kobuk dunes, mainly through its effects on vegetation cover.

The activity and extent of the ISS is probably controlled by a combination of windiness, soil temperature, active-layer thickness, vegetation cover, soil moisture during the snow-free season, and by snow cover during the rest of the year (Neuman, 1993; Mann et al., 2002a; Wolfe, 2006). This suite of conditions co-occur under a windy climate that is dry and cold in winter, and dry and sunny in summer – the same conditions inferred to have prevailed in northern Alaska during ice-age stadials (Guthrie, 2001; Mann et al., 2013). Thus the dune-field core of the ISS was probably most active during cold, dry times when sand sheets expanded outwards across the site of the Carter Section, and loess over-passed the site to be deposited farther to the southwest. At the height of interstadials when climate was less windy, wetter in summer, and snowier in winter, the ISS tended to stabilize, and its fringing sand sheets retreated northwards. Loess fallout then dominated at the site of the Carter Section, enhanced by the increased cover of dust-trapping vegetation (Muhs et al., 2003a; Jensen et al., 2016). During the warmest, wettest interstadials, aeolian deposition declined enough to allow full-scale soil development accompanied by peat accumulation, colonization by woody shrubs, and the growth of epigenetic ice wedges.

5.2. Paleo-environmental history

Based on the preceding inferences about the sources of aeolian sediment and the role of climate in controlling the rate and style of aeolian deposition at the Carter Section, we can interpret the stratigraphy in terms of paleo-environments occurring at the site over the last 37 ka (Fig. 13).

5.2.1. Late Pleistocene: 38 to 18.4 ka

Floodplain aggradation ending shortly before 37.4 ka deposited 22 m of water-lain, sandy sediment at the base of the Carter Section (Fig. 13). By analogy with rapid episodes of floodplain aggradation during the Pleistocene-Holocene transition (Mann et al., 2010), this aggradational interval probably occurred during an interstadial, possibly Greenland Interstadial 8 (GI-8) (Rasmussen et al., 2014). Further support for this inference comes from the organic-rich soils that began development ca. 36.3 ka in the lower part of the main loess unit (Fig. 13).

Moving forward in time, the lower aeolian sand unit in the CS-A section was probably deposited by sand sheets and coppice dunes developed on a point bar of the ancient Titaluk River. The floodplain had ceased aggrading by this time, which may have been a response to cooling climate and/or to a lessening of dune activity in the ISS. If the lower sand-sheet unit is indeed of local origin, its sparse vegetation and sand-dominated sediment provides only a

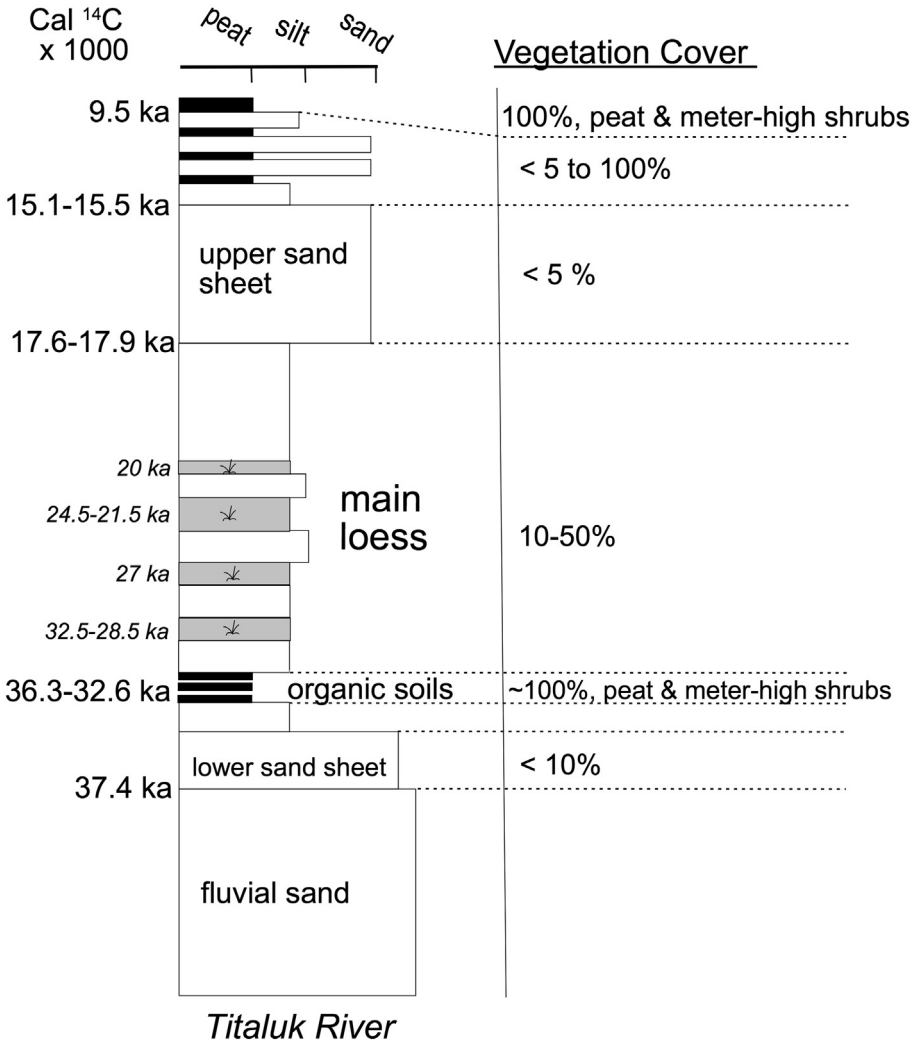

Fig. 13. Summary of paleoenvironmental changes at the site of the Carter Section.

localized glimpse into regional paleoenvironment between 36 and 37.4 ka.

The 13-m-thick, main loess unit deposited between ca. 37 and 17.6 ka comprises the bulk of CS-A (Figs. 9 and 13). Three prominent buried soils associated with epigenetic ice wedges and ice-wedge pseudomorphs date to between 36.3 and 32.6 ka (Fig. 11). The presence of epigenetic ice wedges and the fact these soils possess O and B horizons suggest aeolian deposition episodically fell to low rates during this period. The presence of peat and woody shrub remains indicate the presence of continuous vegetation cover including upright shrubs, which is similar to the vegetation growing near the site today. These vegetation and soil characteristics indicate the climate was relatively warm and moist, an interpretation consistent with the presence of the ice-wedge pseudomorphs.

In the main loess deposit overlying the three buried soils (Fig. 9), there are only minor fluctuations in % OC, % IC, rate of OC accumulation, and the accumulation rates of mineral material (Fig. 10). Percent OC values suggest vegetation cover varied from ~10% to as much as 50%. Particularly abundant plant remains, in some cases including small, woody shrubs, occur at levels in CS-A with estimated ages of ca. 32.5–28.5 ka, ca. 27 ka, ca. 24.5–21.5 ka, and ca. 20 ka, suggesting warmer, wetter conditions occurred at these times (Fig. 13). The occurrence of sand-rich layers containing fewer plant remains than levels above and below suggest that expansions of the ISS occurred between 27 and 24 ka, and again between 21 and 20 ka. However, the persistence of loess deposition throughout the time of the global LGM (ca. 28–18 ka, Clark et al., 2009) suggests this was not when the ISS was most active during the last 37 ka.

5.2.2. The ISS maximum: ca 18–15 ka

The return to sand-sheet deposition ca. 17.8 ka suggests a major increase in the activity and extent of the ISS. This upper sand-sheet unit is best exposed in CS-B where low % OC and sparse root biomass suggest vegetation cover <5% (Fig. 10). The percentages of both OC and IC decrease with increasing height as the MAR rises, reflecting rapid rates of sedimentation when compared to the underlying loess unit.

5.2.3. The Pleistocene-Holocene transition

At levels dating to ca. 16.7 and 15.3 ka sand-sheet deposits are replaced abruptly by loess, suggesting a reduction in ISS activity. Paleosols developed ca. 13.8, 10.9, and 9.4 ka in CS-D (Fig. 13). Soil-forming processes were interrupted by a resurgence of aeolian activity, possibly during the Younger Dryas, which buried the Middle Soil (Unit 5 in CS-D). An epigenetic ice wedge that developed coevally with this loess burying the Middle Soil thawed before

ca. 9.4 ka during the period when the youngest buried soil was developing (Upper Soil, Unit 6 in CS-D).

5.3. Comparisons with other records

Aeolian deposits spanning the last 37 ka provide unique insights into changes occurring on Arctic landscapes because they literally tell us about the ground that ancient plants and animals lived upon. The challenge lies in assessing how representative the sedimentary and ecological conditions at a single site are for the surrounding region. This representative-ness can be assessed in two ways: First by inferring the identities and spatial scales of the sedimentary processes involved, and second by looking for temporal correlations with other paleo-records. In Section 5.1, we identified the dynamics of the ISS as the likely controller of sedimentation in the post-36 ka portions of the Carter Section. The extent and activity of the ISS was in turn probably controlled by climatic factors affecting effective moisture and active-layer depth, which influenced the density of sand-anchoring vegetation cover, which controlled sand availability. In this section, we compare the sequence of paleo-environments at the Carter Section with events elsewhere in the Western Arctic to assess whether the Carter Section is telling us about regional paleo-environments or only about local ones.

5.3.1. Comparisons with non-aeolian records

The development of multiple, organic-rich soils between 36.3 and 32.6 ka in CS-C coincided with warm, moist interstadial conditions recorded in pollen records from Siberia (Müller et al., 2010; Lozhkin and Anderson, 2011) and probably corresponding to Greenland Interstadials GI-5, GI-6, and GI-7 (Rasmussen et al., 2014). The transition from sand sheet to loess occurring in ca. 16.7 and ca.15.3 ka in CS-B and in CS-D coincides with the beginning of GI-1, which in northern Alaska and Siberia saw the northward spread of shrubs (Oswald et al., 1999) and in some areas trees (Müller et al., 2010). At this same time in the Brooks Range, glaciers were in retreat (Balascio et al., 2005; Briner and Kaufman, 2008; Badding et al., 2013; Pendleton et al., 2015), while in the western Brooks Range lake levels were rising and summers warming (Mann et al., 2002b; Kurek et al., 2009; Abbott et al., 2010; Finkenbinder et al., 2015). Development of organic-rich soils ca. 13.8, 10.9, and 9.4 ka in the CS-D section coincided with periods of reduced sea-ice cover and warmer temperatures in the Western Arctic as inferred from isotope values in ancient willow wood from the North Slope (Epstein, 1995; Gaglioti et al., 2017). These same warm, moist periods during the Pleistocene-Holocene transition saw rapid floodplain aggradation along the Titaluk and Ikpikpuk Rivers, paludification in the Arctic Foothills, northward expansion of cottonwood trees (*Populus balsamifera* L.), and widespread permafrost thaw (Mann et al., 2002b, 2010; Gaglioti et al., 2014). The stabilization of the ISS implied by the near-cessation of loess rain at the Carter Section after ca. 9.5 ka coincided with the onset of widespread paludification in the Arctic Foothills of the North Slope (Mann et al., 2002b).

5.3.2. Comparisons with other aeolian records

Kanevskiy et al. (2011) and Lapointe et al. (2017) described the palynology, organic carbon content, $\delta^{18}O$, and cryogeology of a yedoma section exposed along the Itkillik River 150 km southeast of the Carter Section. Multiple, organic-rich paleosols there indicate that interstadial conditions occurred between ca. 36 and 32 ka at the same time organic-rich paleosols developed at the Carter Section. Based on the general stratigraphy of the Itkillik Section, Lapointe et al. (2017) infer that glacial conditions developed gradually after ca. 30 ka and persisted until ca. 18 ka, after which climate became warmer and moister. The Carter Section records a different history, with maximum activity and extent of the ISS being delayed until the interval ca. 18–15 ka (Fig. 13). This difference in the timing of the "aeolian LGM" at the two sites probably relates to their different sediment sources. Instead of receiving aeolian sediment from an upwind sand sea like the ISS, the Itkillik Section received loess entrained from the floodplains of rivers transporting glacial outwash out of the Brooks Range. It follows that the Itkillik Section tracks glacial/deglacial events in the Brooks Range, while the Carter Section reflects the ISS' responses to changing climate conditions on the Arctic Coastal Plain.

Near Fairbanks, 650 km south of the Carter Section, multiple paleosols occur in loess derived from glacial outwash carried by the Tanana River. These soils date to 39–36 ka, 35.5–33.7, and 33.5–31.5 ka (Hamilton et al., 1988; Begét et al., 1990; Berger, 2003; Muhs et al., 2003b) and correlate with the buried soils described in CS-C at the Carter Section. Also in the Fairbanks area, Jensen et al. (2016) reconstructed 150-ka of loess accumulation near Halfway House. They found accumulation rates reached minima during times of peak warmth and cold, with abrupt increases in loess accumulation during periods of rapid climate change. Differences in temporal resolution, sedimentary processes, and aeolian entrainment processes defy meaningful comparisons between the Halfway House and the Carter Section records.

In the Tuktoyuktuk Lowlands some 900 km east of the Carter Section, dunes and sand sheets were widespread between ca. 30 and 13 ka, with small areas of active sand sheets persisting until ca. 8 ka (Bateman and Murton, 2006). Based on limiting dates from two separate sections, a change from predominantly sand dune to sand-sheet deposition occurred between 16.1 and 14.5 ka, which coincided with the sand sheet to loess transition occurring at the Carter Section ca. and ca. 16.8 in CS-D and 15.3 ka in CS-B.

At Zagoskin Lake, 1000 km southwest of the Carter Section on the Yukon-Kuskokwim delta, loess deposition peaked ca. 30 ka, 27–24 ka, and again ca. 18 ka (Muhs et al., 2003b). As in the case of the Itkillik Section, the aeolian source deposits for Zagoskin Lake were primarily glacial outwash. As Muhs et al. (2003b) emphasize, correlations between aeolian deposits can only be expected in cases where sedimentary sources and processes are shared.

Some 2000 km from the Carter Section along the Kolyma River in northeastern Siberia, the Mother of all Yedoma Sections, Duvanny Yar, contains a 50-ka record of loess accumulation (Murton et al., 2015). Paleosol 4 at Duvanny Yar dates between 44 and 36 ka, and Paleosol 5 dates between ca. 35 and 30 ka, making it coeval with the three paleosols described in CS-C. Duvanny Yar is silt-dominated and does not show the alternation of loess and sand-sheet deposition occurring at the Carter Section. At Duvanny Yar, loess sedimentation ceased at 17–15.5 ka, while at the Carter Section the upper sand sheet was succeeded by loess deposition around the same time, ca. 16.8 ka and 15.3 ka. These changes may have occurred in response to the same regional, climatic drivers acting on geomorphologically different sources of aeolian sediment.

5.3.3. Timing of maximum extent of the ISS

If the global LGM occurring between 28 and 18 ka was the coldest, driest interval of the last ice age, then why did the ISS not expand southwards over the Carter Section then? Instead, the Carter Section record indicates the maximum extent of the ISS occurred later, between ca. 18 and 15 ka when the northern hemisphere ice sheets were in retreat (Dyke et al., 2002; Clark et al., 2009; Menounos et al., 2017). We hypothesize that the ISS maximum lagged the global LGM for two reasons. First, dune stabilization tends to have a higher climatic threshold than activation because shifting sands discourage plants from reestablishing. This creates a hysteresis loop where once activated, a dune field may

stay active even though the climate returns to the same state that previously accompanied a vegetated, stabilized dune field (Kocurek and Ewing, 2005).

Secondly, we speculate this hysteresis effect was amplified in the case of the ISS by the role of active-layer depth in controlling sand mobilization (Section 5.1.2). When warmer summers cause active layers to deepen, the soil dries out, plant growth is compromised, sandy soils are no longer anchored by vegetation, and sand movement increases. Thus the optimal time for large-scale sand dune activation in the ISS may be during the initial transition from the coldest, driest conditions of the LGM (dune field already activated) to the warmer, moister conditions of the Bølling-Allerød and Holocene (active layers deepen; blowing sand delays colonizing vegetation). As far as we know, there are no sufficiently precise chronologies available from other Arctic dunefields during Late Pleistocene times to test this hypothesis through regional comparisons.

6. Conclusions

The Carter Section records changes in the extent and activity of the Ikpikpuk Sand Sea (ISS) on Alaska's North Slope between 37 and 9 ka (Fig. 13). Alternations between loess and sand sheet deposition at the margin of the ISS reflect local expressions of global climate changes. The timing of changes between sand sheet and loess deposition at the Carter Section correlate with the chronostratigraphy of other yedoma sections including Duvanny Yar in Siberia, with pollen records of vegetation change in Siberia and Alaska, and with glacier and lake-level fluctuations in the Brooks Range. Times of non-agreement between the Carter Section record and the limited number of other aeolian records available from the region can be explained as differences in dating resolution and sediment sources.

The lower part of the Carter Section records the aggradation of a sparsely vegetated, sandy floodplain prior to 37 ka, possibly during the lengthy GI-8 interstadial. Sand sheets covered the area briefly before ca. 36 ka, after which loess began to accumulate on an upland landscape. Several periods of soil development, peat accumulation, widespread woody vegetation, and permafrost thaw occurred between 36.3 and 32.6 ka under relatively warm, moist climate conditions probably correlative with GI-5, GI-6, and GI-7. Loess deposition resumed thereafter on a landscape supporting 10–50% vegetation cover. Sand sheet and sand dunes along with minimal vegetation cover returned between 18 and 15 ka, recording the maximum expansion of the ISS, which probably began under cold, dry conditions during the LGM but peaked later as warming air temperatures increased active-layer depths and caused effective moisture to decline. The Late Glacial saw alternations between sand-sheet, peat, and loess deposition, with increased sand-sheet activity possibly occurring during the Younger Dryas chronozone.

Unlike today, aeolian processes played major parts in ecosystem structure and function during the Pleistocene on the North Slope. In stark contrast to today, ice age soils lacked organic horizons except during occasional interstadials, and vegetation cover was usually sparse, non-woody, and frequently disturbed by a combination of aeolian erosion and deposition. The spatial and temporal distributions of aeolian deposits have left behind strong legacies in Arctic Alaska in terms of the distribution of ground ice, thermokarst features, and the carbon stored in permafrost.

Acknowledgements

The Bureau of Land Management and the National Science Foundation (Award 1417611 funded this work. We thank Dan Cross-Call and Andrew Weller for assistance in the field. Lola Oliver helped with carbon and nitrogen analyses. Frank Urban provided the wind data. B.V.G. designed the research, executed the fieldwork, supervised all laboratory analyses, and wrote the paper. D.H.M. designed the project, executed the fieldwork, and wrote the paper. P.G. executed the field work and helped with interpretation and writing. M.L.K supplied invaluable field support and interpretation. L.M.F. executed fieldwork and analyzed surficial geology of the study area. R.E.R. conducted initial fieldwork and helped with interpretation. B.M.J. supplied laboratory support and helped with interpretation. M.J.W. supplied laboratory facilities. This is LDEO contribution #8177.

Appendix A. Supplementary data

Supplementary data related to this article can be found at https://doi.org/10.1016/j.quascirev.2018.01.002.

References

Abbott, M.B., Edwards, M.E., Finney, B.P., 2010. A 40,000-yr record of environmental change from Burial Lake in Northwest Alaska. Quat. Res. 74, 156–165.
Ashley, G.M., Hamilton, T.D., 1993. Fluvial response to late Quaternary climatic fluctuations, central Kobuk Valley, northwestern Alaska. J. Sediment. Res. 63, 814–827.
Badding, M.E., Briner, J.P., Kaufman, D.S., 2013. ^{10}Be ages of late Pleistocene deglaciation and neoglaciation in the North-central Brooks range, arctic Alaska. J. Quat. Sci. 28, 95–102.
Balascio, N.L., Kaufman, D.S., Briner, J.P., Manley, W.F., 2005. Late Pleistocene glacial geology of the okpilak-kongakut rivers region, northeastern Brooks range, Alaska. Arctic Antarct. Alpine Res. 37, 416–424.
Bateman, M.D., Murton, J.B., 2006. The chronostratigraphy of Late Pleistocene glacial and periglacial aeolian activity in the Tuktoyaktuk Coastlands, NWT, Canada. Quat. Sci. Rev. 25, 2552–2568.
Baughman, C.A., Mann, D.H., Verbyla, D.L., Kunz, M.L., 2015. Soil surface organic layers in Arctic Alaska: spatial distribution, rates of formation, and microclimatic effects. J. Geophys. Res.: Biogeosciences 120, 1150–1164.
Begét, J.E., Stone, D.B., Hawkins, D.B., 1990. Paleoclimatic forcing of magnetic susceptibility variations in Alaskan loess during the late Quaternary. Geology 18, 40–43.
Berger, G.W., 2003. Luminescence chronology of Late Pleistocene loess-paleosol and tephra sequences near Fairbanks, Alaska. Quat. Res. 60, 70–83.
Bhatt, U.S., Walker, D.A., Raynolds, M.K., Comiso, J.C., Epstein, H.E., Jia, G., Gens, R., Pinzon, J.E., Tucker, C.J., Tweedie, C.E., Webber, P.J., 2010. Circumpolar Arctic tundra vegetation change is linked to sea ice decline. Earth Interact. 14, 1–20.
Blaauw, M., 2010. Methods and code for "classical" age-modelling of radiocarbon sequences. Quat. Geochronol. 5, 512–518.
Black, R.F., 1951. Aeolian deposits in Alaska. Arctic 11, 89–111.
Blott, S.J., Pye, K., 2001. GRADISTAT: a grain size distribution and statistics package for the analysis of unconsolidated sediments. Earth Surf. Process. Landforms 26, 1237–1248.
Brigham-Grette, J., Melles, M., Minyuk, P., 2007. Overview and significance of a 250 ka paleoclimate record from El'gygytgyn Crater Lake, NE Russia. J. Paleolimnol. 37, 1–16.
Briner, J.P., Kaufman, D.S., 2008. Late Pleistocene mountain glaciation in Alaska: key chronologies. J. Quat. Sci. 23, 659–670.
Brock, F., Higham, T., Ditchfield, P., Bronk Ramsey, C., 2010. Current pretreatment methods for AMS radiocarbon dating at the Oxford Radiocarbon Accelerator Unit (ORAU). Radiocarbon 52, 103–112.
Carter, L.D., 1981. A Pleistocene sand sea on the alaskan arctic coastal plain. Science 211, 381–383.
Carter, L.D., 1988. Loess and deep thermokarst basins in Arctic Alaska. In: Proceedings of the Fifth International Conference on Permafrost, pp. 706–711.
Carter, L.D., Galloway, J.P., 1993. Late Pleistocene stabilization and reactivation of eolian sand in northern Alaska: implications for the effects of future climatic warming on an eolian landscape in continuous permafrost. In: Proceedings, Sixth International Conference on Permafrost, pp. 78–83.
Clark, P.U., Dyke, A.S., Shakun, J.D., Carlson, A.E., Clark, J., Wohlfarth, B., Mitrovica, J.X., Hostetler, S.W., McCabe, A.M., 2009. The last glacial maximum. Science 325, 710–714.
Dinter, D.A., Carter, D.L., Brigham-Grette, J., 1990. Late Cenozoic geological evolution of the Alaskan North Slope and adjacent continental shelves. In: Grantz, A., Johnson, L., Sweeney, J.F. (Eds.), The Arctic Ocean Region. The Geology of North America c L. Geological Society of America, Boulder, CO, pp. 459–490.
Dyke, A.S., Andrews, J.T., Clark, P.U., England, J.H., Miller, G.H., Shaw, J., Veillette, J.J., 2002. The Laurentide and Innuitian ice sheets during the last glacial maximum. Quat. Sci. Rev. 21, 9–31.
Epstein, S., 1995. The isotopic climatic records in the Alleröd-Bølling-Younger Dryas and post-Younger Dryas events. Global Biogeochem. Cycles 9, 557–563.

Farquharson, L.M., Mann, D.H., Grosse, G., Jones, B.M., Romanovsky, V.E., 2016. Spatial distribution of thermokarst terrain in Arctic Alaska. Geomorphology 273, 116–133.
Finkenbinder, M.S., Abbott, M.B., Finney, B.P., Stoner, J.S., Dorfman, J.M., 2015. A multi-proxy reconstruction of environmental change spanning the last 37,000 years from Burial Lake, Arctic Alaska. Quat. Sci. Rev. 126, 227–241.
Folk, R.L., 1966. A review of grain-size parameters. Sedimentology 6, 73–93.
French, H.M., 2013. The Periglacial Environment. John Wiley & Sons.
Gaglioti, B.V., Mann, D.H., Jones, B.M., Pohlman, J.W., Kunz, M.L., Wooller, M.J., 2014. Radiocarbon age-offsets in an arctic lake reveal the long-term response of permafrost carbon to climate change. J. Geophys. Res. Biogeosci. 119, 1630–1651.
Gaglioti, B.V., Mann, D.H., Wooller, M.J., Jones, B.M., Wiles, G.C., Groves, P., Kunz, M.L., Baughman, C.A., Reanier, R.E., 2017. Younger-Dryas cooling and sea-ice feedbacks were prominent features of the Pleistocene-Holocene transition in Arctic Alaska. Quat. Sci. Rev. 169, 330–343.
Galloway, J.P., Carter, L.D., 1993. Late holocene longitudinal and parabolic dunes in northern Alaska: preliminary interpretations of age and paleoclimatic significance. United States Geol. Surv. Bull. 2068, 3–11.
Guthrie, R.D., 2001. Origin and causes of the mammoth steppe: a story of cloud cover, woolly mammal tooth pits, buckles, and inside-out Beringia. Quat. Sci. Rev. 20, 549–574.
Hamilton, T.D., Craig, J.L., Sellmann, P.V., 1988. The Fox permafrost tunnel: a late Quaternary geologic record in central Alaska. Geol. Soc. Am. Bull. 100, 948–969.
Hinzman, L.D., Bettez, N.D., Bolton, W.R., Chapin, F.S., Dyurgerov, M.B., Fastie, C.L., Griffith, B., Hollister, R.D., Hope, A., Huntington, H.P., Jensen, A.M., Jia, G.J., Jorgenson, T., Kane, D.L., Klein, D.R., Kofinas, G., Lynch, A.H., Lloyd, A.H., McGuire, A.D., Nelson, F.E., Oechel, W.C., Osterkamp, T.E., Racine, C.H., Romanovsky, V.E., Stone, R.S., Stow, D.A., Sturm, M., Tweedie, C.E., Vourlitis, G.L., Walker, M.D., Walker, D.A., Webber, P.J., Welker, J.M., Winker, K.S., Yoshikawa, K., 2005. Evidence and implications of recent climate change in northern Alaska and other arctic regions. Climatic Change 72, 251–298.
Hopkins, D.M., 1982. Aspects of the paleogeography of beringia during the late Pleistocene. In: Hopkins, D.M., Matthews, J.V., Schweger, C.E., Young, S.B. (Eds.), Paleoecology of Beringia, pp. 3–28.
Jensen, B.J., Evans, M.E., Froese, D.G., Kravchinsky, V.A., 2016. 150,000 years of loess accumulation in central Alaska. Quat. Sci. Rev. 135, 1–23.
Jiilavenkatesa, A., Dapkunas, S.J., Lum, L.H., 2001. Particle Size Characterization. US Department of Commerce Report.
Kanevskiy, M., Shur, Y., Fortier, D., Jorgenson, M.T., Stephani, E., 2011. Cryostratigraphy of Late Pleistocene syngenetic permafrost (yedoma) in northern Alaska, Itkillik River exposure. Quat. Res. 75, 584–596.
Kocurek, G., Ewing, R.C., 2005. Aeolian dune field self-organization—implications for the formation of simple versus complex dune-field patterns. Geomorphology 72, 94–105.
Kocurek, G., Lancaster, N., 1999. Aeolian system sediment state: theory and Mojave Desert Kelso dune field example. Sedimentology 46, 505–515.
Koster, E.A., Dijkmans, J.W., 1988. Niveo-aeolian deposits and denivation forms, with special reference to the great Kobuk Sand Dunes, Northwestern Alaska. Earth Surf. Process. Landforms 13, 153–170.
Kurek, J., Cwynar, L.C., Ager, T.A., Abbott, M.B., Edwards, M.E., 2009. Late Quaternary paleoclimate of western Alaska inferred from fossil chironomids and its relation to vegetation histories. Quat. Sci. Rev. 28, 799–811.
Lapointe, L., Talbot, J., Fortier, D., Fréchette, B., Strauss, J., Kanevskiy, M., Shur, Y., 2017. Middle to late wisconsinan climate and ecological changes in northern Alaska: evidences from the Itkillik River yedoma. Palaeogeogr. Palaeoclimatol. Palaeoecol. 485, 906–916.
Lea, P.D., 1990. Pleistocene periglacial eolian deposits in southwestern Alaska: sedimentary facies and depositional processes. J. Sediment. Res. 60, 582–591.
Lea, P.D., Waythomas, C.F., 1990. Late-Pleistocene eolian sand sheets in Alaska. Quat. Res. 34, 269–281.
Lozhkin, A.V., Anderson, P.M., 2011. Forest or no forest: implications of the vegetation record for climatic stability in Western Beringia during Oxygen Isotope Stage 3. Quat. Sci. Rev. 30, 2160–2181.
Mann, D.H., Heiser, P.A., Finney, B.P., 2002a. Holocene history of the Great Kobuk sand dunes, northwestern Alaska. Quat. Sci. Rev. 21, 709–731.
Mann, D.H., Peteet, D.M., Reanier, R.E., Kunz, M.L., 2002b. Responses of an arctic landscape to Lateglacial and early Holocene climatic changes: the importance of moisture. Quat. Sci. Rev. 21, 997–1021.
Mann, D.H., Groves, P., Reanier, R.E., Kunz, M.L., 2010. Floodplains, permafrost, cottonwood trees, and peat: what happened the last time climate warmed suddenly in arctic Alaska? Quat. Sci. Rev. 29, 3812–3830.
Mann, D.H., Groves, P., Kunz, M.L., Reanier, R.E., Gaglioti, B.V., 2013. Ice-age megafauna in Arctic Alaska: extinction, invasion, survival. Quat. Sci. Rev. 70, 91–108.
Menounos, B., Goehring, B.M., Osborn, G., Margold, M., Ward, B., Bond, J., Clarke, G.K.C., Clague, J.J., Lakeman, T., Koch, J., Caffee, M.W., 2017. Cordilleran Ice Sheet mass loss preceded climate reversals near the Pleistocene Termination. Science 358, 781–784.
Miller, G.H., Alley, R.B., Brigham-Grette, J., Fitzpatrick, J.J., Polyak, L., Serreze, M.C., White, J.W., 2010. Arctic amplification: can the past constrain the future? Quat. Sci. Rev. 29, 1779–1790.
Muhs, D.R., Ager, T.A., Been, J., Bradbury, J.P., Dean, W.E., 2003a. A late Quaternary record of eolian silt deposition in a maar lake, St. Michael Island, western Alaska. Quat. Res. 60, 110–122.
Muhs, D.R., Ager, T.A., Bettis, E.A., McGeehin, J., Been, J.M., Begét, J.E., Pavich, M.J., Stafford, T.W., De Anne, S.P., 2003b. Stratigraphy and palaeoclimatic significance of Late Quaternary loess–palaeosol sequences of the Last Interglacial–Glacial cycle in central Alaska. Quat. Sci. Rev. 22, 1947–1986.
Müller, S., Tarasov, P.E., Andreev, A.A., Tütken, T., Gartz, S., Diekmann, B., 2010. Late Quaternary vegetation and environments in the Verkhoyansk Mountains region (NE Asia) reconstructed from a 50-kyr fossil pollen record from Lake Billyakh. Quat. Sci. Rev. 29, 2071–2086.
Murton, J.B., 1996. Morphology and paleoenvironmental significance of Quaternary sand veins, sand wedges, and composite wedges, Tuktoyaktuk coastlands, western Arctic Canada. J. Sediment. Res. 66, 17–25.
Murton, J.B., 2001. Thermokarst sediments and sedimentary structures, Tuktoyaktuk Coastlands, western Arctic Canada. Global Planet. Change 28, 175–192.
Murton, J.B., Bateman, M.D., 2007. Syngenetic sand veins and anti-syngenetic sand wedges, Tuktoyaktuk Coastlands, western Arctic Canada. Permafr. Periglac. Process. 18, 33–47.
Murton, J.B., Goslar, T., Edwards, M.E., Bateman, M.D., Danilov, P.P., Savvinov, G.N., Gubin, S.V., Ghaleb, B., Haile, J., Kanevskiy, M., 2015. Palaeoenvironmental interpretation of yedoma silt (ice complex) deposition as cold-climate loess, Duvanny yar, northeast Siberia. Permafr. Periglac. Process. 26, 208–288.
Nelson, F.E., Hinkel, K.M., Shiklomanov, N.I., Mueller, G.R., Miller, L.L., Walker, D.A., 1998. Active-layer thickness in north central Alaska: systematic sampling, scale, and spatial autocorrelation. J. Geophys. Res. 103, 963–973.
Neuman, C.M., 1993. A review of aeolian transport processes in cold environments. Prog. Phys. Geogr. 17, 137–155.
Newman, J.E., Branton, C.I., 1972. Annual water balance and agricultural development in Alaska. Ecology 53, 513–519.
Osterkamp, T.E., Payne, M.W., 1981. Estimates of permafrost thickness from well logs in northern Alaska. Cold Reg. Sci. Technol. 5, 13–27.
Oswald, W.W., Brubaker, L.B., Anderson, P.M., 1999. Late Quaternary vegetational history of the Howard Pass area, northwestern Alaska. Can. J. Bot. 77 (4), 570–581.
Pendleton, S.L., Ceperley, E.G., Briner, J.P., Kaufman, D.S., Zimmerman, S., 2015. Rapid and early deglaciation in the central Brooks range, arctic Alaska. Geology 43, 419–422.
Ping, C.L., Jastrow, J.D., Jorgenson, M.T., Michaelson, G.J., Shur, Y.L., 2015. Permafrost soils and carbon cycling. Soils 1, 147–171.
Rasmussen, S.O., et al., 2014. A stratigraphic framework for abrupt climatic changes during the Last Glacial period based on three synchronized Greenland ice-core records: refining and extending the INTIMATE event stratigraphy. Quat. Sci. Rev. 106, 14–28.
Reimer, P.J., Bard, E., Bayliss, A., Beck, J.W., Blackwell, P.G., Bronk Ramsey, C., Buck, C.E., Cheng, H., Edwards, R.L., Friedrich, M., 2013. IntCal13 and Marine13 radiocarbon age calibration curves 0-50,000 years cal BP. Radiocarbon 55, 1869–1887.
Reineck, H.E., Singh, I.B., 2012. Depositional Sedimentary Environments: with Reference to Terrigenous Clastics. Springer-Verlag.
Wahrhaftig, C., 1965. Physiographic Divisions of Alaska. US Government Printing Office.
Walker, D.A., Jia, G.J., Epstein, H.E., Raynolds, M.K., Chapin III, F.S., Copass, C., Hinzman, L.D., Knudson, J.A., Maier, H.A., Michaelson, G.J., 2003. Vegetation-soil-thaw-depth relationships along a low-arctic bioclimate gradient, Alaska: synthesis of information from the ATLAS studies. Permafr. Periglac. Process. 14, 103–123.
Walker, D.A., Raynolds, M.K., Daniëls, F.J., Einarsson, E., Elvebakk, A., Gould, W.A., Katenin, A.E., Kholod, S.S., Markon, C.J., Melnikov, E.S., 2005. The circumpolar Arctic vegetation map. J. Veg. Sci. 16, 267–282.
Walker, D.A., Kuss, P., Epstein, H.E., Kade, A.N., Vonlanthen, C.M., Raynolds, M.K., Daniëls, F.J., 2011. Vegetation of zonal patterned-ground ecosystems along the North America Arctic bioclimate gradient. Appl. Veg. Sci. 14, 440–463.
Washburn, A.L., 1980. Permafrost features as evidence of climatic change. Earth Sci. Rev. 15, 327–402.
Wendler, G., Shulski, M., Moore, B., 2010. Changes in the climate of the alaskan North Slope and the ice concentration of the adjacent Beaufort sea. Theor. Appl. Climatol. 99, 67–74.
Westhoff, V., Van Der Maarel, E., 1978. The Braun-blanquet Approach. Springer.
Wolfe, S.A., 2006. High-latitude Dune Fields. Encyclopedia of Quaternary Sciences. Elsevier Publishing, pp. 599–607.
Zhang, T., Osterkamp, T.E., Stamnes, K., 1996. Some characteristics of the climate in northern Alaska, USA. Arctic Alpine Res. 28, 509–518.